Universidade de Aveiro

Departamento de Física

2019

CAROLINA MATEUS EIRAS BERNARDO

SENSIBILIDADE DO WRF AO TIPO DE SUPERFÍCE E PARAMETRIZAÇÃO DA CANÓPIA URBANA DURANTE UM EVENTO DE ONDA DE CALOR EM ESTOCOLMO

WRF SENSITIVITY TO LAND USE AND URBAN CANOPY MODEL DURING A HEAT WAVE EVENT IN STOCKHOLM

Universidade de Aveiro

2019

Departamento de Física

CAROLINA MATEUS EIRAS BERNARDO

SENSIBILIDADE DO WRF AO TIPO DE SUPERFÍCE E PARAMETRIZAÇÃO DA CANÓPIA URBANA DURANTE UM EVENTO DE ILHA DE CALOR EM ESTOCOLMO

WRF SENSITIVITY TO LAND USE AND URBAN CANOPY MODEL DURING A HEAT WAVE EVENT IN STOCKHOLM

Tese apresentada à Universidade de Aveiro para cumprimento dos requisitos necessários à obtenção do grau de Mestre em Ciências do Mar e da Atmosfera, realizada sob a orientação científica do Doutor Alfredo Rocha, Professor Associado c/ Agregação no Departamento de Física da Universidade de Aveiro, e co-orientação da Doutora Ana Cristina Carvalho, investigadora no SMHI – Swedish Meteorological and Hidrolgical Institute.

o júri

President

Prof. Doutor José Manuel Henriques Castanheira

Professor Auxiliar do Departamento de Física da Universidade de Aveiro

Prof. João Carlos Andrade dos Santos

Professor Auxiliar com Agregação do Departamento de Física da Universidade de Trás-os-Montes e Alto Douro.

Doutora Ana Cristina Caldeira da Silva Carvalho

Investigadora no SMHI – Swedish Meteorological and Hydrological Institute

agradecimentos

Quero agradecer em especial aos meus orientadores, Professor Doutor Alfredo Rocha e Doutora Ana Cristina Carvalho por todo o apoio e disponibilidade demonstrado, determinantes na elaboração deste trabalho.

Gostaria também de agradecer aos meus colegas de curso e do grupo de Atmosfera pela amizade e por sempre estarem disponíveis para ajudar. Ao Luís Carvalheiro por todo o apoio técnico prestado na compilação e implementação do modelo.

Por fim quero agradecer aos meus pais, por sempre me terem incentivado a progredir na minha vida académica e por sempre me terem apoiado.

palavras-chave Onda de calor, clima urbano, WRF, uso do solo, canópia urbana, ilha de calor urbano, Estocolmo.

Resumo

As ondas de calor estão entre os mais perigosos fenómenos de tempo extremo, sendo que num cenário de alterações climáticas, a frequência da sua ocorrência está projetada para aumentar significativamente na Europa. Zonas densamente urbanizadas, como as cidades, estão mais vulneráveis a eventos de temperaturas extremas do que as zonas rurais envolventes devido ao efeito de ilha de calor urbano pré-existente. O presente trabalho pretende avaliar a sensibilidade do modelo WRF aos dados do uso do solo e à parametrização da canópia urbana, durante um evento de ilha de calor, na região de Estocolmo. Para o teste de sensibilidade ao uso do solo foram utilizadas três base de dados diferentes. Os resultados mostraram que uma base de dados mais atualizada e com uma maior resolução aumentam a performance do modelo nos campos do vento e da temperatura. Para o teste de sensibilidade às parametrizações da canópia urbana, foram comparadas duas simulações produzidas com o acoplamento de dois modelos de parametrização da canópia urbana (UCM) diferentes, o *Single Layer Urban Canopy Model* (SLUCM) e o *Building Effect Parametrization Model* (BEP), utilizando uma base de dados de uso do solo de alta resolução, com três categorias urbanas diferentes. Os resultados mostraram que estes modelos dependem significativamente dos parâmetros utilizados para descrever a geometria e as propriedades da cidade, contudo, o uso do modelo BEP permitiu melhorar a simulação das componentes u e v, enquanto que para o campo da temperatura, os resultados não apresentaram diferenças significativas.

keywords Heat wave, urban climate, WRF, landuse, urban Canopy, urban heat island, Stockholm.

abstract

Heatwaves are among the most dangerous extreme weather events, and their occurrence is projected to significantly increase over Europe in a climate change scenario. Densely urbanized regions as cities, are more vulnerable to extreme hot weather events, than rural areas, due to pre-existing UHI effect. The present work evaluates the WRF model sensitivity to landuse and *Urban Canopy Model* (UCM) parametrizations, during a heat wave event occurring in Stockholm region. The landuse sensitivity test compares the model results produced with three different landuse datasets, showing that using a more updated and high-resolution dataset increases the model skill simulating wind and temperature fields. The UCM sensitivity, compared the model performance coupled with two UCMs, SLUCM and BEP model, using a high resolution landuse dataset with three different urban categories. The simulated results showed that these models are strongly dependent on the parameters used by each model to describe the city geometry and proprieties, besides this, using the BEP model increased the model skill simulating the u and v wind components, but the differences found for the temperature field were insignificant.

CONTENTS

LIST OF FIGURES

LIST OF TABLES

1 Introduction

The thin layer of the atmosphere that is directly influenced by the presence of the Earth's surface is called atmospheric boundary layer (ABL) (Oke et al. 2017). It plays a central role in the exchange of heat, moisture, momentum, trace gases and aerosols between land, ocean and ice surfaces, in cloud formation, and in the general circulation of the atmosphere. This layer responds to surface forcings like frictional drag, evaporation and transpiration, heat transfer, pollutant emission, and terrain induced flow modification, with a timescale of about an hour or less (Stull, 1988). The ABL is typically 1 or 2 km thick, but it can be quite variable in time and space, ranging from tens of meters to a few kilometers or more. This stable layer traps turbulence, pollutants, and moisture below it and prevents most of the surface friction from being felt by the free atmosphere (Wallace and Hobbs, 2006).

The land surface nature has an important role governing the ABL characteristics, controlling the exchanges of energy mass and momentum. It is the nature of the Earth surface that determines the quantity of absorbed, reflected and emitted radiation, the transformations of energy and mass, by transforming radiant energy in thermal energy and water in water vapor, the interceptions of precipitation and air pollutants and the deflection and slowing of the wind (Oke et al., 2017).

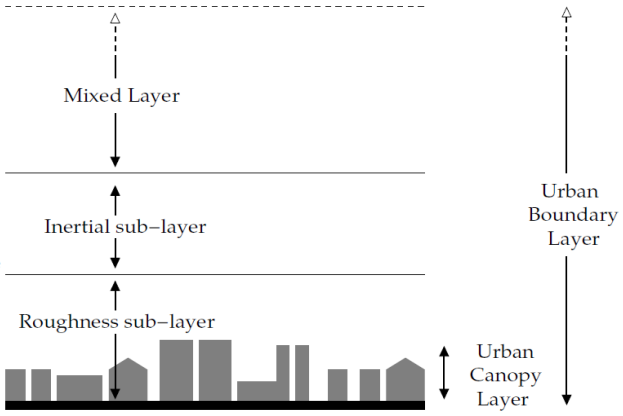

Figure 1- Schematic of the UBL with the configuration of the sub-layers described by Oke et al., 2017. Figure adapted from Malakooti, 2010.

The process of urbanization changes radically the nature of the surface and atmospheric properties of a region, as it changes the radiative, thermal, moisture and aerodynamic characteristics. Large cities have different land surface characteristics from the surrounding rural areas, such as larger buildings that produce a stronger drag on the wind, less ground moisture and vegetation, resulting in reduced evaporation, different

albedo characteristics that are strongly dependent on the relationship between sun position and alignment of the urban street canyons, different heat capacity and greater emissions of *pollutants and* anthropogenic heat production (Wallace Hobbs, 2006). These differences are responsible for modifying the ABL over a large city, forming the Urban boundary layer (UBL) with distinct characteristics from the surrounding rural ABL. Oke et al. (2017) divide this layer in 4 sub-layers, Figure 1 illustrates the configuration of these sub-layers. The urban canopy layer (UCL) is the bottom layer of the UBL, and it is located between the surface and the mean height of buildings/trees. The roughness sub-layer (RSL) includes the UCL and extends up to two to five times the height of buildings/trees. It is the layer where the flow responds to the roughness of the individual elements. The inertial sublayer (ISL) corresponds to the top of the surface layer (SL), which includes the UCL, the RSL and the ISL. Finally, there is the mixed layer (ML), above the ISL where the proprieties of the atmosphere are uniformly mixed by thermal turbulence and usually trapped by a capping inversion.

The city centers are usually hotter than the surroundings rural areas. This phenomenon is called the urban heat island effect (UHI) and is one of the clearest and best documented examples of the interaction between the local climate and the urbanized surfaces in the cities. The greatest temperature differences between rural and urbanized areas are observed during the night. Cities with a population of about 1000 inhabitants can experience a maximum temperature difference of 2 to 3 ºC, and cities with more than a million can experience a maximum temperature difference of 8 to 12 ºC (Stull, 1988).

The UHI effect makes cities more vulnerable to extreme hot weather events than the rural areas (Li & Bou-Zeid, 2013). Heat waves are an example of this type of events. There is no universal definition for heat wave (Meehl and Tebaldi, 2004, Perkins and Alexander, 2013, Robinson, 2001), but it can be generally described as a period of consecutive days where conditions are hotter than normal (Perkins et al., 2012). A heat wave typically results from large-scale, stagnant, high pressure systems that produce a temporal temperature anomaly over an entire region. These events are among the most dangerous of natural hazards and can cause a heavy toll on human systems, affecting health, livelihoods and infrastructure. It has been associated with rise of the mortality rates, especially within risk groups. For example, the heat wave events that occurred in Europe in the summer of 2003 (Robine et al., 2008; Trigo et al.,2005) and in the Russian Federation in July and August 2010 (Grum, 2011, Osborn, 2010) had had devastating effects, associated with tens of thousands heat related deaths, extreme wildfires, and severe drought.

The Fifth Assessment Report (AR5) of Working Group I of the Intergovernmental Panel on Climate Change (IPCC, 2013) refer an observed increase, since 1950, in the intensity and durations of heat waves in large areas of Europe, Asia and Australia, as well as an increase in the number of warm days and nights. It also showed that, by the end of this century, it is very likely that heat wave frequency and duration will continue to increase. It is also important to note that, globally, there is more people living in urban areas than in rural areas. Nowadays, more than 50% of the world populations live in urban areas and this percentage is projected to reach 68% by the middle of the XXI century (United Nations, 2018).

Moreover, possible interactions have been investigated between UHI and heat waves. Li and Bou-Zeid (2013) used a combination of observational, numerical and analytical analyses to study these interactions and found that the UHI effect can be amplified during a heat wave event.

The combination of the previous factors makes especially important the comprehension of Cities' responses to hot weather events and their influence in urban climates. The Urban SIS is a project developed by the Swedish Meteorological and Hydrological Institute as part of a Copernicus proof-of-concept project from 2015–2018 ("UrbanSIS – Climate Information for European Cities", 2019). Its main goal was to dynamic downscaling to the urban level (1 × 1 km^2) a set of atmospheric essential climate variables (ECVs) and impact indicators, related to flooding events, heatwaves and air pollution episodes, to be used to support the infrastructure and health sectors operating in cities. The downscaling of the historical period was performed with the HARMONIE model, forced by UERRA-ALADIN reanalysis for the historical period, and by data derived from the GLOBAQUA project, for three European cities, Stockholm, Bologna and Rotterdam.

1.1 Objectives of the study

The main objective of the present study is the investigation of the urban effects occurring in the UBL in Stockholm, during a heat wave event. In particular, the UHI effect is investigated and the development of PBL is studied, as well as the 2-m temperature and 10-m wind speed. This study is based on numerical model simulations performed with Weather Research and Forecasting (WRF) model, which were assessed with meteorological observations from surface stations. The WRF model performance is evaluated by performing sensitivity tests to land use and UCM. More detailed information on the model simulations and observational data can be found in section 2.

1.2 State of the art

As previously mentioned, the Earth's surface properties play an important role controlling the atmospheric dynamics within the ABL. The landuse is a very important parameter which describes different proprieties of the land surface. For accurate modelling of the urban meteorological fields, the use of appropriate landuse data is needed. During the last decades, improvements in satellite technology made possible the acquisition of high-resolution landuse data which could be used as lower boundary conditions in numerical models.

The impact of different landuse datasets in numerical model simulations was widely studied. In 2004, Pineda et al. (2004) adapted the Coordination of information on the Environment Land Cover landuse data edition referring to the year 2000 (CORINE 2000) over a mountainous region in Iberian Peninsula to be used in the fifth-generation Pennsylvania State University/NCAR Mesoscale Model (MM5). With the new estimation of

the soil parameters the authors carried out a comparison between two numerical simulations, one with the adaptation of CORINE landuse and new physical parameters, and the other with the default USGS (United States Geological Survey) data processed to be used with MM5. The results showed clear local differences between the two simulations, although when comparing with ground observations the improvements in the model performance were not evident.

López-Espinoza et al. (2012) studied the impacts of urban growth in temperature in central Mexico from 1993 to 2009, based on observations and two simulations performed with the WRF. The simulations were performed using two different landuse datasets, the USGS (from 1992-93) dataset and the landuse dataset from the National Institute of Statistics and Geography in Mexico (INEGI-2019), both with a resolution of 30 seconds. The results obtained showed an increase of temperature in the studied area when using the INEGI-2009 dataset which better represents the landuse. Also, Cheng el al. (2013) compared the use of three different landuse datasets in the WRF model for Taiwan, showing the importance of using an accurate landuse dataset when studying simulated temperature, wind speed, surface heat flux components and land-sea breeze dynamics.

In the last few decades, a remarkable effort was put on numerical simulations in order to improve the representation of the thermal and aerodynamic effects occurring in urban areas. In particular, the WRF model has been vastly used to study urban effects in the cities. The first approach used in mesoscale models to introduce the urban effects consisted in representing the urban areas as flat surfaces with modified soil constants and parameters, to account for the large heat storage of the cities, and with high roughness length (Salamanca et al., 2011). However, this approach didn't consider the heterogeneities present in urban surfaces leading to the development of the urban canopy models (UCM).

Kusaka et al. (2001) and Kusaka and Kimura (2004) developed a single layer urban canopy model (SLUCM) that recognizes the three-dimensional nature of the cities by representing their surface as infinite long street canyons with three urban surfaces (walls, roofs, and roads). This model represents the shadowing, trapping and multiple reflection of solar radiation and consider an exponential wind profile in a two-dimensional street canyon. It also calculates the surface temperature based on the surface energy budget, estimate the friction velocity and canyon drag coefficient and includes the anthropogenic heat release.

Other UCMs generally used to study urban effects in the boundary layer is the building effect parametrization (BEP) model, developed by Martilli et al. (2002). The BEP is a multi-layer model which interacts directly with the ABL. It recognizes the three-dimensional nature of urban surfaces and the fact that buildings vertically distribute sources and sinks of heat, moisture, and momentum through the whole urban canopy layer, which substantially impacts the thermodynamic structure of the urban roughness sub-layer and the lower part of the urban boundary layer. The BEP model considers the impact of horizontal (roofs and streets) and vertical (walls) urban surfaces when calculating the momentum, heat and turbulent kinetic energy fluxes passed to the ABL. It also considers shadowing, reflection, and trapping of shortwave and longwave radiation in the street canyons but doesn't take into account the anthropogenic heat.

UCMs have been widely used to study the effects occurring in urban regions. Lin et al. (2008) studied the WRF model performance simulating this effect over northern Taiwan.

In that work, the authors used the WRF model coupled with the single layer UCM to study the impacts of the UHI in the development of the ABL and in the land-sea breeze circulation. The authors also studied the model sensitivity to the UCM model parameters by increasing heat capacity, thermal conductivity, albedo, roughness length for momentum and roughness length for heat of roofs, walls and street for double values and to the anthropogenic heat. The results showed that the simulations using the UCM improved the prediction of the UHI effect, the boundary layer development and the land sea breeze. The results of the sensitivity tests showed that the anthropogenic heat is especially important for ABL development and UHI intensity, especially during nighttime and early morning when compared with the other parameters.

Kim et al. (2013) studied the WRF model sensitivity to the PBL parametrization over the region of Paris. They used the two PBL parametrizations that giving the best results against observational data, to produce new simulations with the single layer UCM and the CORINE landuse dataset. The model results applying the CORINE land use and the UCM showed that this setting represented better the meteorological fields, particularly the wind speed which is improved below 1000 m height. The authors also concluded that using the UCM and the CORINE landuse data has a greater influence on meteorological fields than the use of different PBL schemes.

The accuracy of the UCM depends, in part, in the parameters that represent the morphologic characteristics of the cities (Loridan et al. 2010). He et al. (2019) developed a high-resolution gridded dataset of UCM parameters for the city of Beijing. The new dataset was incorporated in the WRF model coupled whit three different UCMs to investigate the influence of the new parameters. The results of the study showed that the high-resolution parameters usually have more accurate representation of the diurnal and horizontal distributions of 2-m surface air temperature and 10-m wind speed, especially when using the BEP model.

Additionally, using satellite observations of surface skin temperature (T_{skin}), Zhang et al. (2017) examined the UHI effect for two inner land cities, with different city population and buildings densities, Oklahoma City and Xi'an City in China. The authors found a stronger UHI effect in Xi'an, which is smaller but has a larger population and building density, suggesting that factors like population density, building density and city size are important factor in determining this effect.

2 Methodologies and Data

This section starts with a description of the study domain and the selection of the study period. After this, all the observational datasets used in this work are presented, and their characteristics described. Following this, the model settings are explained, and finally the methodology to evaluate the model data against observations is presented.

2.1 Study area and period

The area of interest of this study is Stockholm, in Sweden, and its surrounding areas. Stockholm is the capital of Sweden and is the most populous city in Scandinavia, with a population of about 1.5 million people living within the urban area.

It is located on the east coast of the country, over an archipelago and between the Baltic Sea to the east and Lake Mälaren to the west (Figure 2).

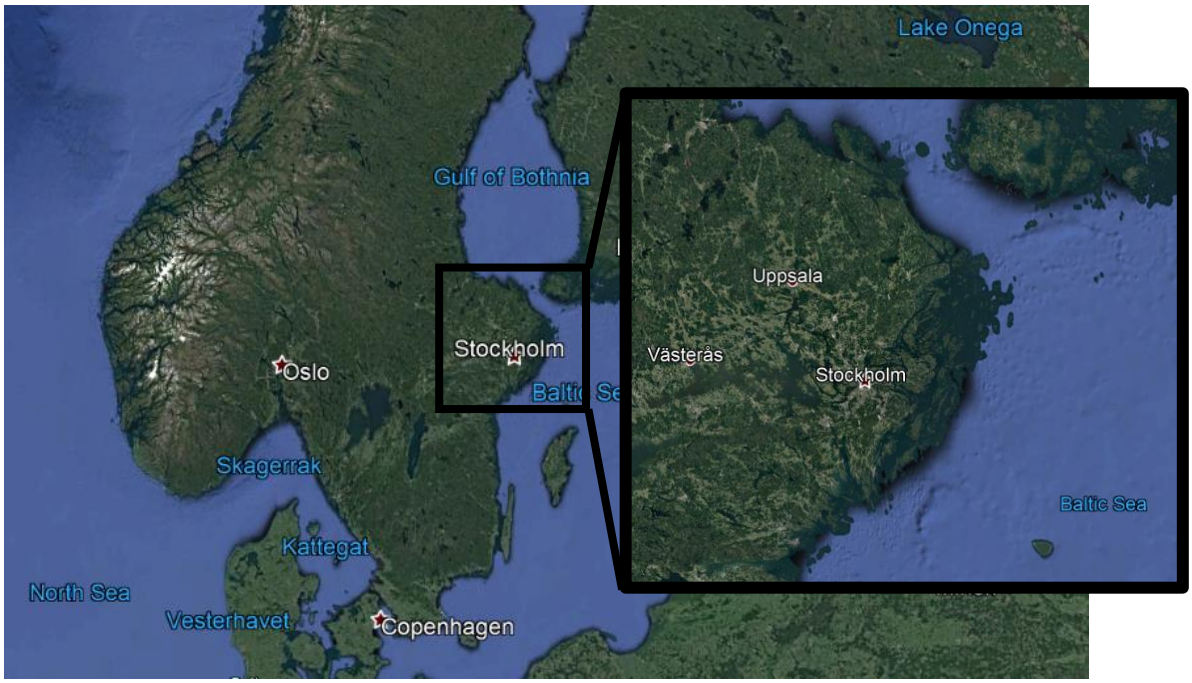

Figure 2 – Map of Sweden, with a zoom in the studied area, Stockholm. Source: Google Earth Pro.

As previously mentioned, this study aims to investigate the performance of WRF model in the region of Stockholm during a heat wave event, its sensitivity to the landuse dataset and to the urban canopy models used. Given this, a period of particularly warm weather was considered during the 2014' Summer. This period occurred during the months of July and August 2014 which were unusually hot in Sweden, with a strong and influence of a persistent high-pressure system (Figure 3a).

Several stations in the country recorded historical values of mean and maximum temperatures. They reached temperatures above 20ºC and 30 ºC, respectively, leading to the firsts SMHI warnings for high temperatures in several regions of the country (SMHI). Stockholm was one of these areas. Figure 3b shows the daily mean and maximum temperature in Stockholm A station, located in the city center during the months of July and August.

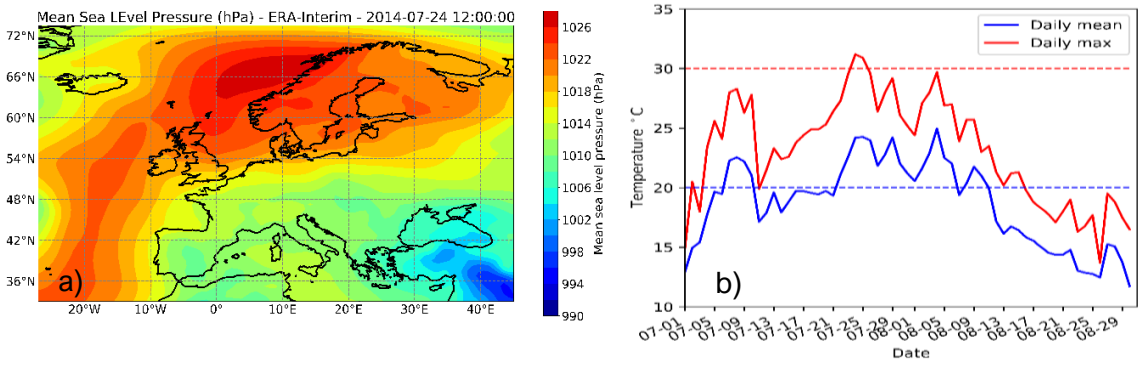

Figure 3 - a) Mean sea level pressure (hPa) from Era-Interim reanalysis for the 24th July at 12:00 UTC and b) Stockholm A station daily mean and maximum temperatures for the months of July and August 2014 .

Figure 4 shows the normalized temperature anomaly in Stockholm A station, for the Summer months. The temperature anomaly was greatest during the last's days of July and the firsts of August, with maximum positive anomalies around 0.4 ºC.

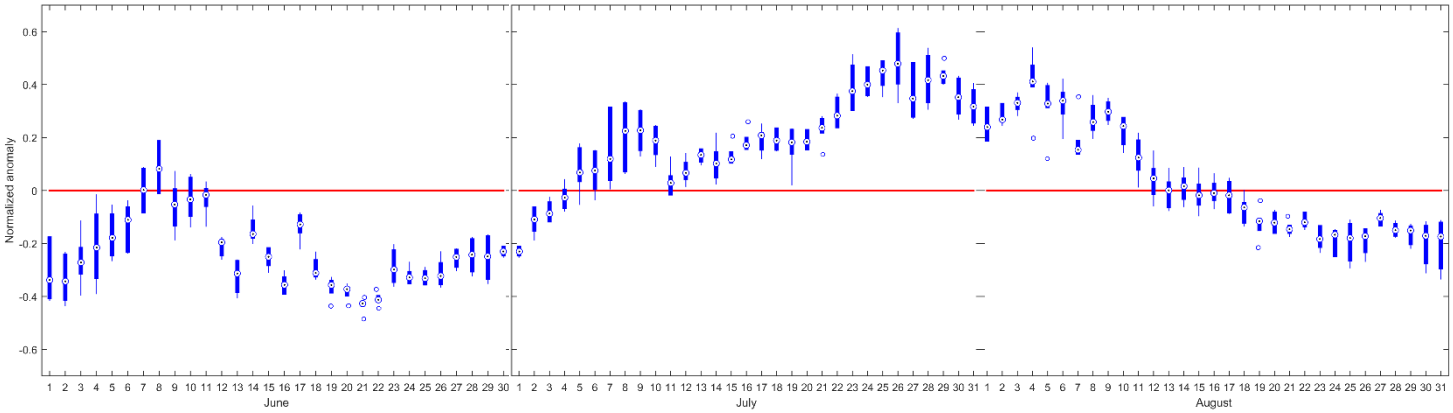

Figure 4 – 2 meters temperature normalized anomaly for Summer months, June, July and August relative to the year of 2014 in the station Stockholm A.

The summer season is climatologically characterized by a well-defined high-pressure system centered over Azores islands, whose influence can extend over central Europe and by a low-pressure system over Island. Over north Africa is possible to note a thermal low-pressure system as well as in middle east (Figure 5a). On the other hand, the MSLP anomalies of the period between the 21st of July and the 10th of August, in Figure 5b, show that this period was characterized by a stronger high-pressure system over Russia, and it's also clear a weakening and southern migration of Azores high and the Island low pressure systems.

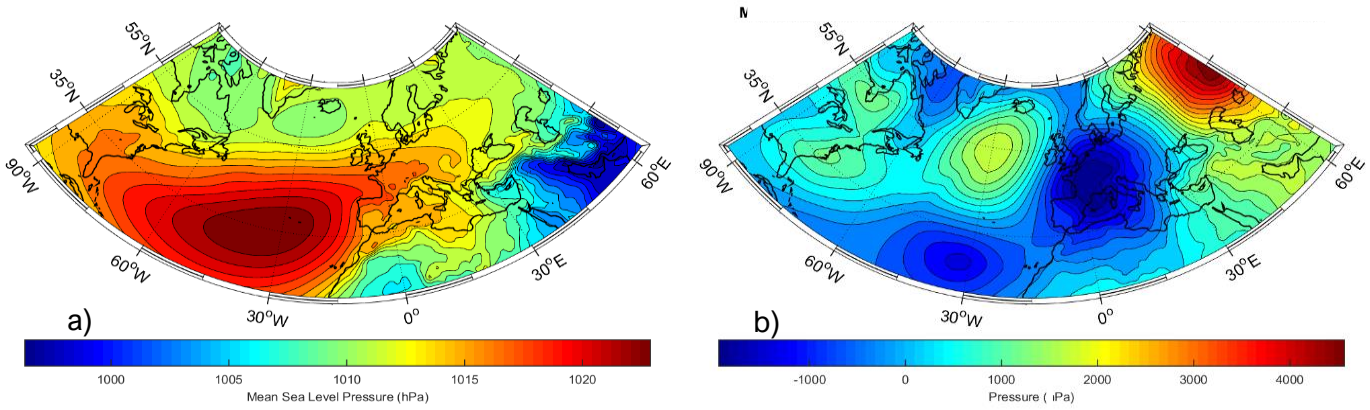

Figure 5 a) –Mean Sea Level Pressure data from Era-Interim, averaged over the Summer months, June, July and August between 1979 and 2016 and b) Mean Sea Level Pressure anomaly for the period between 21st Of July and 11th of August relative to the Summer's average between 1979 and 2016.

Given this, this study focus the period between the 21st of July and the 8th of August. Figure 6 shows the temperature and wind hourly time series in Bromma Airport station, during this period.

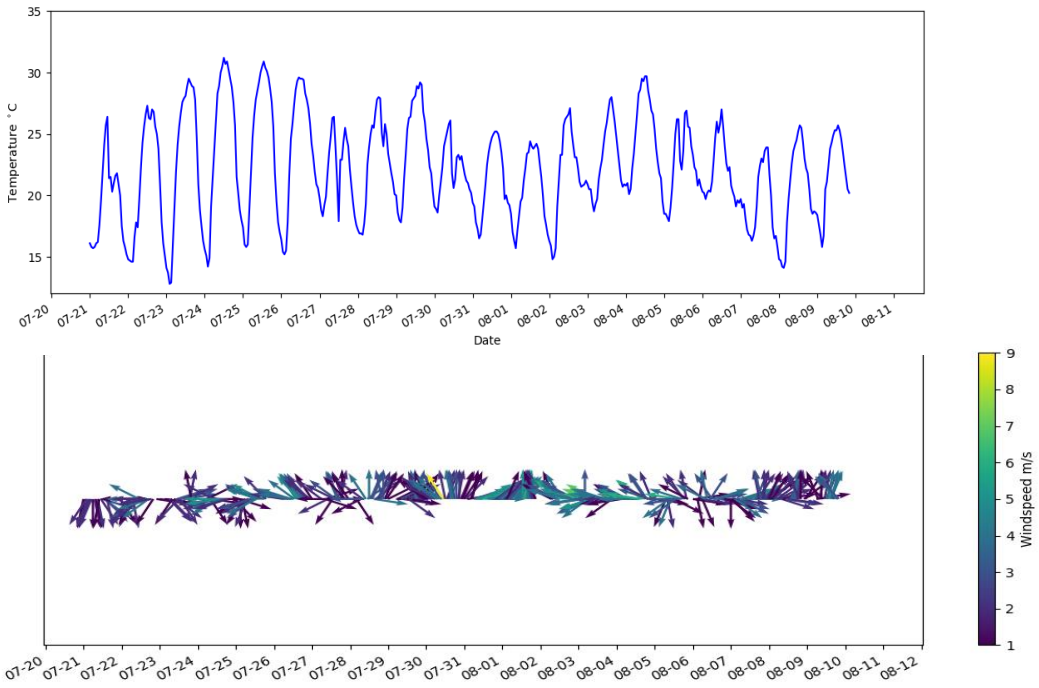

Figure 6 –2-m Temperature (top) and 10-m wind speed and direction (bottom) time series in Bromma station, for the period between the 21st of July and the 8th of August 2014.

2.2 Observational Data

Different observational datasets were used in this work. ERA-interim reanalysis data from the European Center for Medium-range Weather Forecasts (ECMWF) was used to initialize the meteorological fields and to specify boundary conditions in the model simulations. Era-Interim data set has a spatial resolution of approximately 80 km (T255 spectral) on 60 vertical levels from the surface up to 0.1 hPa. Regarding the sea surface temperature (SST) field, the daily, high-resolution (1/12º), real-time, global, sea surface temperature data (RTG_SST) analysis, from the National Centers for Environmental Prediction/Marine Modeling and Analysis Branch (NCEP / MMAB) was used to initialize the SST field in the model. The data was downloaded for the months of July and August 2014 from the NCEP website (ftp://polar.ncep.noaa.gov/pub/history/sst/rtg_high_res/).In order to evaluate the model performance, two observational datasets were used. First, the E-OBS dataset (Haylock et al., 2008) version 17.0 was used. This dataset is based on the ECA&D (European Climate Assessment and Data) station data set and other archives and is available for download at ECA&D website (https://www.ecad.eu/download/ensembles/download.php), where the meteorological variables were retrieved namely, daily mean, maximum and minimum surface temperatures and mean seal level pressure on a 0.25º regular lat-lon grid.

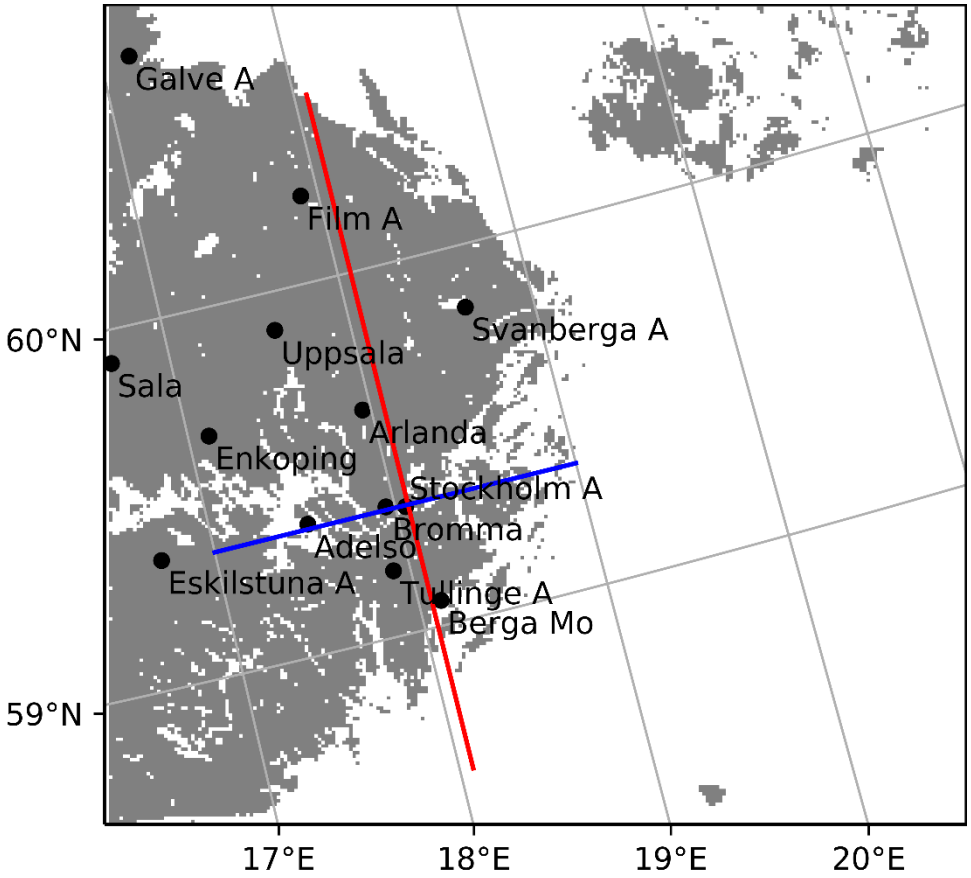

Figure 7 – Location of the meteorological stations. Red line represent the location of the N-S and the blue line represent the W-E cross-sections considered in this work.

The second dataset used to validate the model performance was the meteorological data from the Swedish Meteorological and Hydrological Institute (SMHI) stations. The hourly values of temperature at 2 meters and wind speed and direction at 10 meters, from 13 stations located within Stockholm region and the surrounding areas (Figure 7) were downloaded from the SMHI website (https://www.smhi.se/data/meteorologi/ladda-ner-meteorologiska-observationer).

2.3 Model simulations

The numerical simulations used in this work were produced with the Advanced Research Weather and Forecasting model (ARW) version of the WRF system. The WRF-ARW model is a numerical weather prediction (NWP) and atmospheric simulation system designed for both research and operational applications, and it's the result of a collaborative effort of several organizations to build a next-generation mesoscale forecast model and data assimilation system. Namely, the National Center for Atmospheric Research's (NCAR) Mesoscale and Microscale Meteorology (MMM) Division, the National Oceanic and Atmospheric Administration's (NOAA) National Centers for Environmental Prediction (NCEP) and Earth System Research Laboratory (ESRL), the Department of Defense's Air Force Weather Agency (AFWA) and Naval Research Laboratory (NRL), the Center for Analysis and Prediction of Storms (CAPS) at the University of Oklahoma,

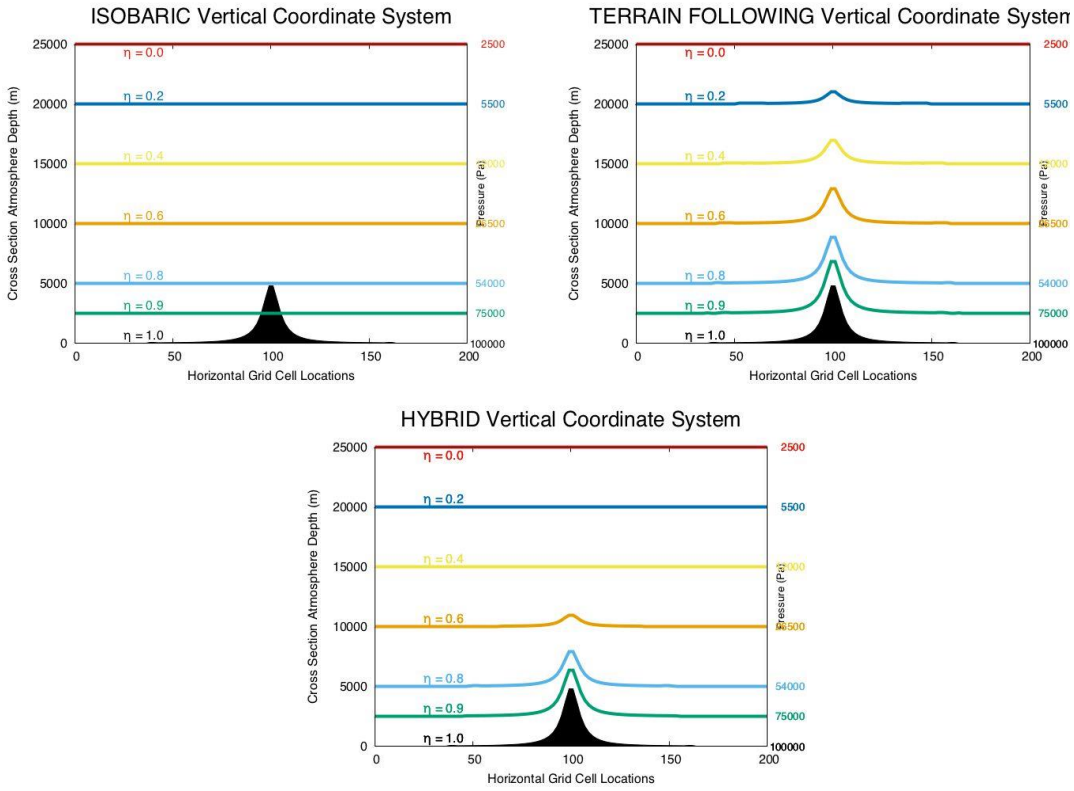

Figure 8 – Vertical coordinate systems in the WRF model. Isobaric (Upper-left), Terrain Following (Upper-right) and Hybrid (bottom). Retrieved from http://www2.mmm.ucar.edu/wrf/users/docs/user_guide_V3.9/ARWUsersGuideV3.9.pdf.

and the Federal Aviation Administration (FAA), with the participation of university scientists (Skamarock et al.,2008).

The simulations in this work were performed with WRF model version 3.9, released in April 2017. This version of WRF model has introduced the possibility of using Hybrid Vertical Coordinates (HVC), which is a coordinate that is terrain following near the ground and then relax towards an isobaric surface aloft (Figure 8). The HVC were developed with the purpose of reducing the artificial influence of the topography towards the top of the model (Wang 2017). In order to take advantage of this new feature in this work, the WRF model was compiled with HVC and this option was activated.

The meteorological data used as initial and boundary conditions was the ERA-interim reanalysis data from ECMWF. The sea surface temperature (SST) data used to initialize the model was the daily, high-resolution (1/12º), real-time, global, sea surface temperature, (RTG_SST), analysis, developed at NCEP/MMAB.

The configuration of the model domain was chosen regarding the main synoptic structures showed in Figure 5. Figure 9 shows a parent domain (d01) with a grid cell resolution of 25 x 25 km, 120 x 90 grid points, centered at 58ºN ,5ºE and two two-away nested domains: the intermediate domain (d02) with a resolution of 5 km x 5 km and 121 x 121 grid points and the inner domain (d03) covering Stockholm region, with 1 × 1 km resolution and 241 × 241 grid points.

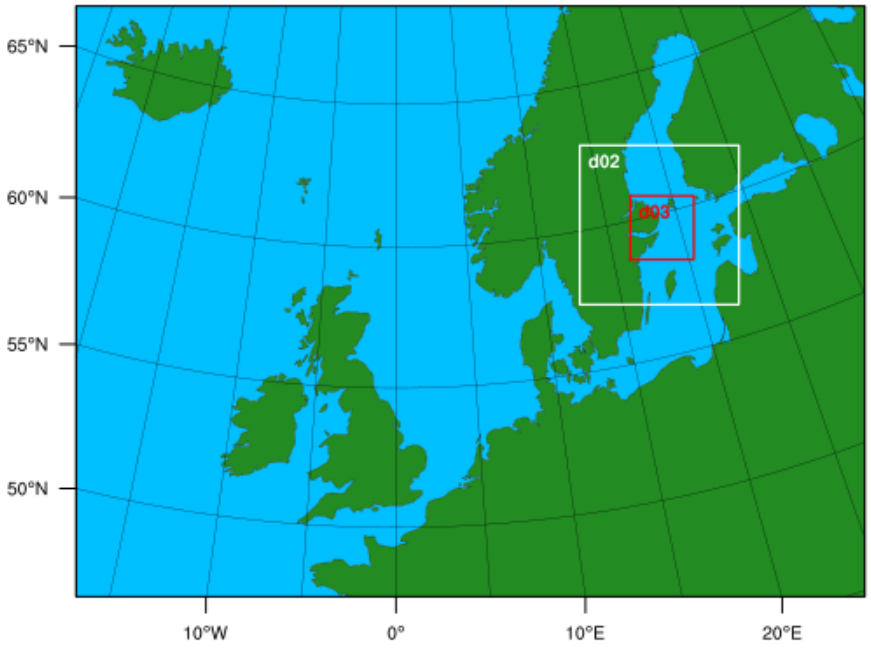

Figure 9 – WRF Model domains used in the simulations.

The model time-step was defined as 6*dx as suggested by Skamarock et al. (2008), where dx is in km and the time-step is in seconds. However, with this fixed time step, the model was getting unstable and crashed after a few hours of simulation. To avoid this, the model was set with an adaptative time-step, which ensures the model stability by adapting

the time-step to the temporally evolving wind fields (u, v and w) and ensuring the model stability in all model domains.

The set of parametrizations used in the model configuration were chosen according with Teixeira (2012), who studied the differences in using different Urban Canopy Models available in the WRF model for the region of Lisbon. For the microphysics scheme it was used the WRF Single-Moment 6-class (Hong and Lim, 2006). In terms of radiation parametrizations, Dudhia shortwave radiation scheme (Dudhia, 1989) and Rapid Radiative Transfer Model (RRTM) longwave radiation model (Mlawer et al., 1997) were specified. For the surface layer option, it was used the Revised MM5 Monin-Obukhov scheme (Skamarock et al. 2008), for the land surface parametrization, the Noah Land Surface Model, was used (Chen and Dudhia, 2001). Regarding the boundary layer parametrization, it was used the Bougeault and Lacarrere (BouLac) (Bougeault and Lacarrere, 1989), and for the cumulus parametrization, the Kain-Frisch scheme was used (Kain 2004).

Regarding the lower boundary conditions, three different land use/land cover datasets were tested in the model:

- The USGS land use dataset, generated by the United States Geological survey's (USGS) Earth Resources Observation System (EROS) Data Center, the University of Nebraska-Lincoln (UNL) and the Joint Research Centre of the European Commission, derived from 1-km Advanced Very High Resolution Radiometer (AVHRR) data, spanning between April 1992 and March. This dataset is the default WRF landuse and it distinguishes 24 landuse categories with a 30 s resolution.
- The MODIS landuse dataset, derived from observations spanning a year input of Terra and Aqua data. With 20 land cover classes defined by the International Geosphere Biosphere Programme (IGBP).
- The CORINE Land Cover dataset, version 18, referring the land use / land cover status of year 2012, developed within the European programme Corine Land Cover, coordinated by the European Environment Agency (EEA). This dataset has a minimum width of linear elements of 100 meters and consist in a 44 categories-based classification.

To evaluate the model sensitivity to changes in landuse three simulations were performed, with USGS global 30s (USGS), the Modis 30s (MODIS) and the Corine Landuse 3s datasets (CORINE). The three datasets were specified to domains d02 and d03 of each simulation (table 1). Domain d01 was calculated with USGS 30s data in all simulations performed. In order to incorporate the CORINE Land Cover dataset in the WRF model, this dataset was reclassified to the USGS classification. The Corine Land Cover Classes were reclassified to USGS classes based on the methodology of Pineda et al. (2004), and the 11 CORINE urban classes were reclassified to the 3 USGS urban classes applied in the UCMs, High Density Residential, Low Density Residentials and Commercial/Industrial/Transportation, as applied by Teixeira (2012).

Table 1 – Landuse dataset and Urban Canopy Model used in the simulations.

Simulation Set	Run	Landuse	Urban Canopy Model
Landuse	USGS	USGS 30s	None
	MODIS	Modis 30s	None
	CORINE	Corine 3s	None
Urban Canopy Models	SLUCM	Corine 3s	SLUCM
	BEP	Corine 3s	BEP

Finally, in order to test the model sensitivity to the UCM, two more simulations were performed. The landuse data used in this test was the CORINE dataset, that distinguishes 3 different urban classes used by the UCMs in the simulations. The first simulation of this set was performed using the Single Layer UCM (SLUCM) and the second was performed using the BEP model (BEP) (Table 1). These two simulations were later compared with the CORINE simulation, which is used as a control simulation in this test.

2.4 Model Validation

2.4.1 Domain 01

The validation of the coarser domain (d01) was performed by comparing the model results against the data from the E-OBS dataset. The coarser domain (d01) has a resolution of 25 km, which differs from the E-OBS resolution, therefor the E-OBS data set was interpolated to match the WRF data grid, using a bilinear interpolation. To achieve the model validation, some relevant statistical parameters were calculated according to Fekih and Mohamed (2017) and applied by Senade (2018). First, the Root Mean Squared Error (RMSE) was computed, which represents the deviation between simulated y_i and respective observed o_i data in the same place and time instant and *n* is the total number of data points.

$$RMSE = \sqrt{\frac{1}{n}\sum_{i=1}^{n}(y_i - o_i)^2} \quad (1)$$

If the simulations are perfect ($y_i = o_i$) the RMSE is equal to zero. The RMSE increases through larger positive values as the difference between simulated and observed values increase (Wilks, 2011).

To evaluate the tendency of the data, we calculated the model Bias. The model Bias is simply the difference between the average forecast and the average observation. If the simulations overestimate the observations the Bias is positive (BIAS > 0) and in the other hand, if the simulations underestimate the observations the Bias is negative (BIAS < 0). (Wilks, 2011)

$$Bias = \frac{1}{n}\sum_{i=1}^{n}(y_i - o_i) \tag{2}$$

To evaluate the dispersion of the error between observed and simulated data, the Standard Deviation Error (STDE) was calculated:

$$STDE = \sqrt{\frac{1}{n}\sum_{i=1}^{n}\left((y_i - o_i) - \frac{1}{n}\sum_{i=1}^{n}(y_i - o_i)\right)^2} \tag{3}$$

.

The STDE is the root square of the arithmetic average squared difference between each error and the mean error. STDE low values indicate low dispersion of simulation errors, and high STDE values indicate a high dispersion of errors.

2.4.2 Domain 03

The model domain d03 was compared against 2 meters temperature and 10 meters wind data from the SMHI meteorological stations. To validate this domain, in addition to the RMSE (eq 1), the correlation coefficient (r) and the Standard Deviation of both modeled (S) and observed data (S_{obs}) were computed, and the results presented in Taylor diagrams.

$$r = \frac{\sum(o_i - \bar{o})(y_i - \bar{y})}{\sqrt{\sum(o_i - \bar{o})^2\sum(y_i - \bar{y})^2}} \tag{4}$$

$$S_{obs} = \sqrt{\frac{\sum_{i=1}^{n}(o_i - \bar{o})^2}{N}} \tag{5}$$

$$S = \sqrt{\frac{\sum_{i=1}^{n}(y_i - \bar{y})^2}{N}} \tag{6}$$

3 Results and Discussion

3.1.1 Parent Domain (D01) validation

The parent domain (d01) was first compared against meteorological observations. The E-OBS meteorological grid dataset was used to validate the parent domain (d01) of all simulations. Daily surface mean (T_{mean}), maximum (T_{max}) and minimum (T_{min}) temperature values, as well as the daily mean sea level pressure (P), are available in E-OBS dataset, and were compared with data from d01 obtained in all simulations.

BIAS, RMSE and STDE values for $T_{mean,}$ T_{max} and T_{min} and mean sea surface pressure (P) are presented in

Table 2, Table 3 and Table 4, respectively. It is possible to note a positive bias for the T_{mean} of all simulations. A negative bias was found for the T_{max}, T_{min} and P. The results also showed that the negative bias in T_{max} and T_{min} are very high. The RMSE results shows also showed a better agreement between E-OBS and model data for T_{mean} and P, while the T_{max} and T_{min} presented larger values of RMSE. For the STDE similar results were found, relatively small values for mean variables and big differences in the extremes. Despite this, MODIS simulation shows the best agreement with E-OBS dataset for both mean daily temperature and sea level pressure.

Table 2 –Mean BIAS between E-OBS and simulations over all simulated period.

BIAS	USGS	MODIS	CORINE	UCM	BEP
T_{mean}	0.54	0.47	0.54	0.54	0.54
T_{max}	-19.40	-19.48	-19.42	-19.41	-19.42
T_{min}	-15.91	-15.95	-15.91	-15.90	-15.89
P	-0.33	-0.29	-0.32	-0.32	-0.32

Table 3 - Mean RMSE between E-OBS and simulations over all simulated period.

RMSE	USGS	MODIS	CORINE	UCM	BEP
T_{mean}	1.20	1.16	1.19	1.20	1.19
T_{max}	19.71	19.79	19.73	19.72	19.72
T_{min}	16.40	16.44	16.40	16.39	16.38
P	1.03	1.00	1.02	1.02	1.02

Previous studies have compared E-OBS datasets with datasets interpolated from higher density station network (Kyselý and Plavcová, 2010 and Hofstra and Haylock, 2009). The results found by Hofstra and Haylock 2009, showed that the E-OBS dataset compares better to the mean of the variables of the existing data sets than to the extremes. This, and

the coarse resolution of E-OBS dataset, can have contributed to the high errors found between simulations and this dataset, especially for T_{max} and T_{min}.

Table 4 - Mean STDE between E-OBS and simulations over all simulated period.

STDE	USGS	MODIS	CORINE	UCM	BEP
T_{mean}	0.88	0.87	0.88	0.88	0.87
T_{max}	3.34	3.34	3.34	3.34	3.34
T_{min}	3.87	3.87	3.87	3.87	3.87
P	0.68	0.67	0.68	0.68	0.68

3.2 Landuse sensitivity test

In the WRF model, many of the physical processes that affect air–surface exchanges are a function of land use or land cover. Figure 10 shows the different landuse datasets used in the model simulations namely, USGS, MODIS and CORINE. It's possible to note several differences between the three datasets.

The inner domain (d03) is composed mostly by water grid cells, as it includes the areas of the Baltic Sea surrounding Stockholm and the many lakes over land. The landuse dataset that represents more water grid-cells in d03 is the USGS dataset, with 69.0 % of the total grid-cells corresponding to water, while in the MODIS and CORINE datasets the water grid cells correspond to 61.2 % and 63.3%, respectively.

The land areas of d03 are mostly composed by forest and natural green areas. MODIS is the dataset that represents the larger amount of grid cells with these categories, with 35.8% of forest and natural green areas in the domain, while the USGS and CORINE datasets shows 26.7% and 23.9%, respectively. Cropland and pasture categories are also present in d03. The dataset that represent more grid-cells with these categories is CORINE, with 9.3% of the total grid-cells with these categories, while USGS and MODIS represent 2.8% and 1.1% respectively.

Regarding the urban cover, the dataset that represents more urban grid-cell points in d03, is the CORINE dataset, with 2.1% of the total grid cells corresponding to urban grid cells, while the MODIS datasets has the smallest percentage of urban cover (0.9%). The USGS dataset has an urban grid cell percentage of 1.5 %.

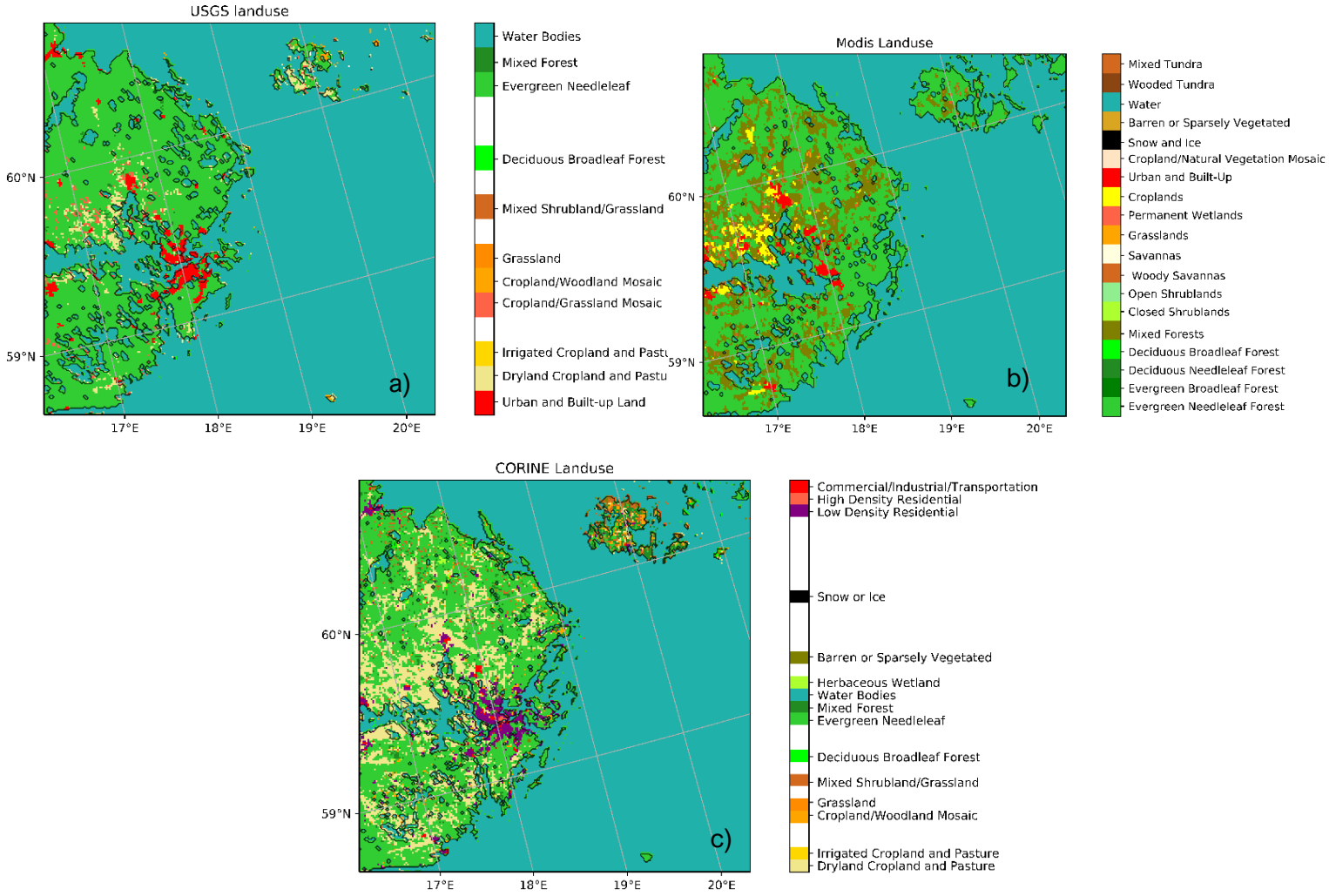

Figure 10 – Land use maps of the inner domain (d03), from a) USGS, b) MODIS and c) CORINE datasets. The black line corresponds to the contour line of the land-sea masked of each dataset.

Table 2 shows the landuse categories of the meteorological station grid-points used in this study. It is possible to note that, in the CORINE dataset the stations grid-points have only *urban* or *cropland and pasture* categories, while in MODIS and USGS datasets, several stations grid-points correspond to *Water* or *Forest* categories. For instance, Stockholm A station location has an urban category in both MODIS and CORINE datasets while the USGS dataset represents this location as water. Bromma station location land use category corresponds to an urban category in both MODIS and CORINE datasets, while in the USGS it corresponds to *Dryland Cropland and Pasture*.

Table 5 – Landuse category of the station's locations grid-points in the USGS, MODIS and CORINE datasets.

Meteorological stations	USGS	MODIS	CORINE
Svanberga A	Water Bodies	Water	Dryland Cropland and Pasture
Berga Mo	Water Bodies	Evergreen Needleleaf	Commercial/Ind/Transport
Uppsala	Cropland/Grassland Mosaic	Croplands	Dryland Cropland and Pasture
Bromma	Dryland Cropland and Pasture	Urban and Built-Up	Commercial/Ind/Transport
Film A	Evergreen Needleleaf	Mixed Forest	Dryland Cropland and Pasture
Galve A	Urban and Built-Up	Woody Savannas	Low Density Residential
Stockholm A	Water Bodies	Urban and Built-Up	High Density Residential
Tullinge A	Evergreen Needleleaf	Evergreen Needleleaf	Commercial/Ind/Transport
Arlanda	Evergreen Needleleaf	Evergreen Needleleaf	Commercial/Ind/Transport
Adelso	Evergreen Needleleaf	Mixed Forest	Dryland Cropland and Pasture
Eskilstuna A	Evergreen Needleleaf	Mixed Forest	Dryland Cropland and Pasture
Enkoping	Cropland/Grassland Mosaic	Mixed Forest	Dryland Cropland and Pasture
Sala	Evergreen Needleleaf	Evergreen Needleleaf	Dryland Cropland and Pasture

3.2.1 2-m Temperature

The temperature near the surface is directly influenced by the characteristics of surface, Figure 11 shows the 2-m temperature distribution for the USGS simulations and the differences between this simulation and MODIS and CORINE simulations, in the 24th of July, 2014 at 00:00 and at 12:00 UTC.

As seen before, this day is included in the period with very high temperatures that had occurred in the region. At 00:00 UTC, the highest temperatures are found over the Baltic Sea and over the lakes, with temperatures ranging between 21ºC and 23 ºC. It's also possible to note some regions inland that are particularly warmer than its surroundings. Comparing these regions distribution with the landuse maps from Figure 10, it's evident that these regions correspond to densely urbanized regions, as Stockholm City center, Arlanda, Uppsala, Gälve, showing the occurrence of nocturnal UHI effect.

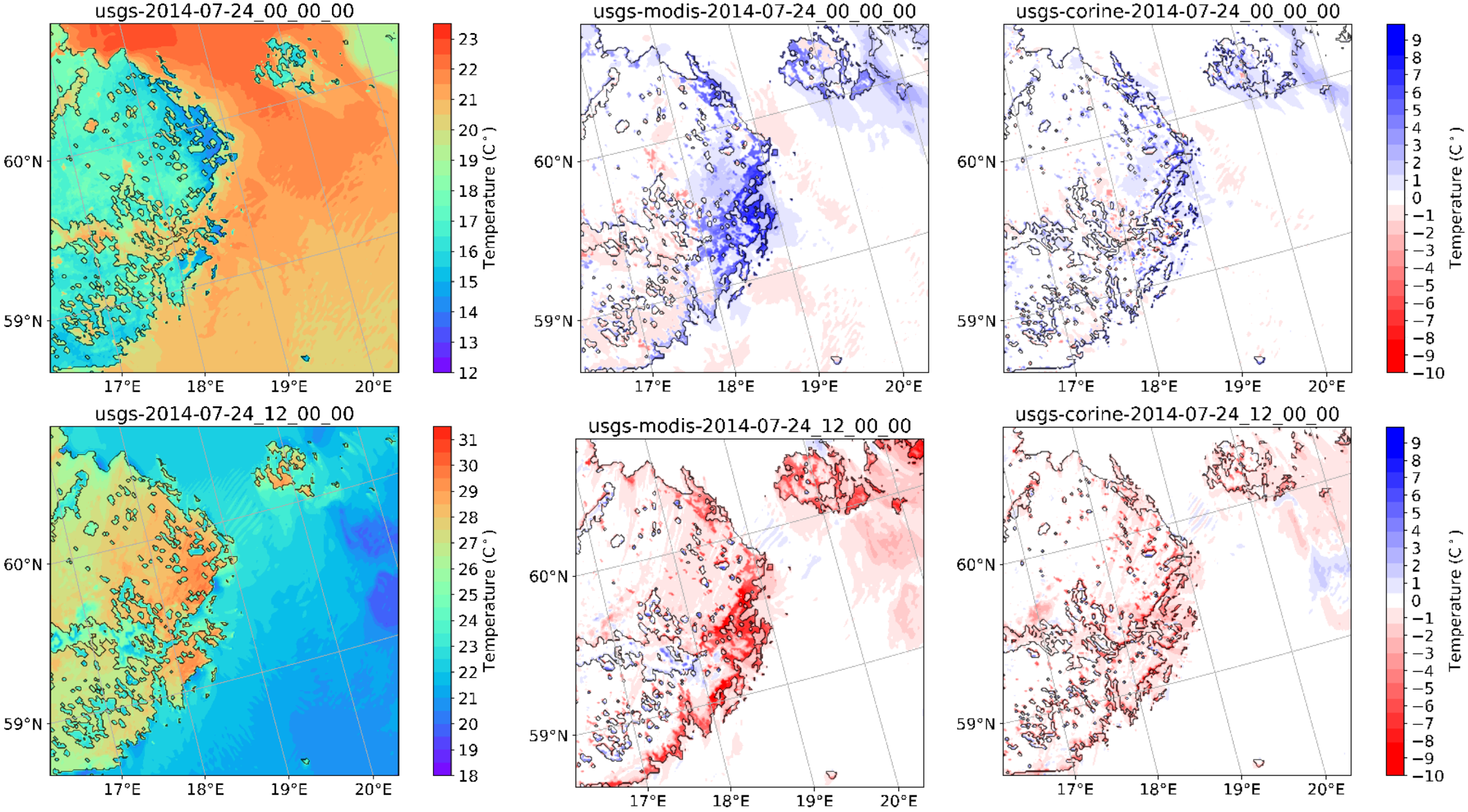

Figure 11 – 2-m temperature spatial distribution for d03 in USGS (left), and diference between USGS and MODIS (center) and CORINE (rigth) simulations, on the 24th of July 2014, at 00:00 (top) and 12:00 (bottom).

At 12:00 UTC, the warmer temperatures are found over land where temperatures are reaching around 30ºC; the lower temperatures are found over the Baltic Sea and lakes present in the domain.

By analyzing the spatial differences between the USGS simulation and the MODIS and CORINE simulations, it's possible to note that the most significant differences are found over land, especially along the coastline and around the lakes, which corresponds to land-sea mask differences between the two simulations. The land-sea mask of CORINE simulation shows more similarities with USGS land-sea mask, than with the MODIS's. Particularly in the coastline regions which results in bigger differences between MODIS and USGS than those found when comparing the USGS and CORINE datasets. Apart from this, the landuse parameters, as the albedo, the soil moisture available, the emissivity, the roughness length and the thermal Inertia, used by the model in CORINE simulation are the same used for USGS simulations, while different parameters where used for MODIS simulation, which can explain the larger differences found over inland regions of the domain when using the MODIS landuse. The parameters used in each dataset are presented in Table 9 and 10 of Annex 1.

During the night period, MODIS and CORINE simulations show lower temperatures along the coastline regions, where USGS represent water and the other simulations represent land. On the other hand, during the day, the USGS simulation show lower temperatures than the two other runs in these regions, as the grid cells represented by land categories in CORINE and MODIS datasets correspond to water grid-cells in USGS dataset.

Figure 12 shows the temporal evolution of 2-m temperature in *Bromma* Airport station, and in the correspondent model grid point for the simulations performed, during the three warmest days recorded during the simulation period. The observations show the maximum daily temperatures around 30ºC, occurring around 12:00 UTC and the minimum daily temperatures around 15ºC, occurring in the first hours of the day. The results show that, during this period, the model underestimates the temperature during the day, and

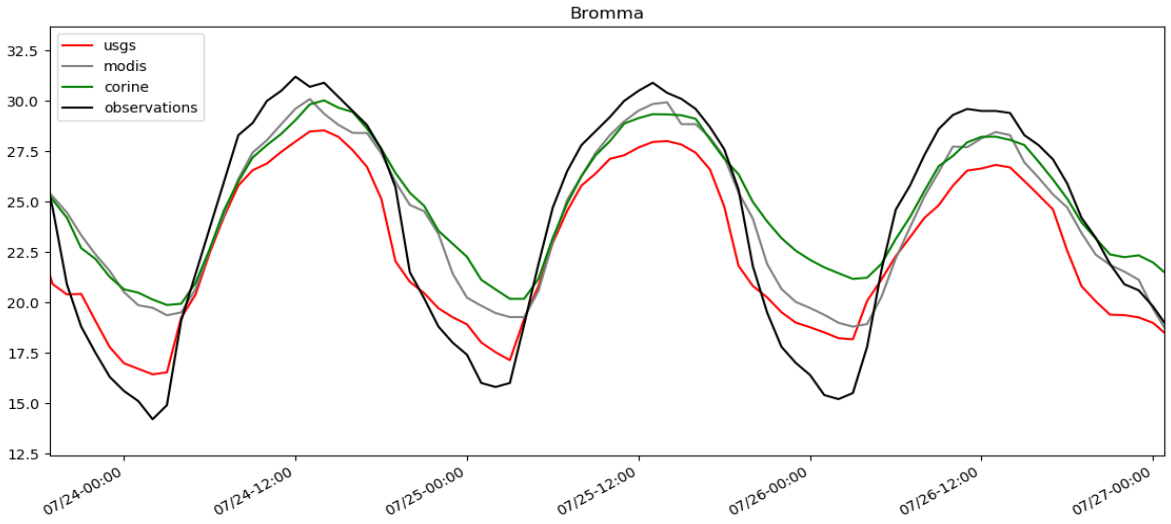

Figure 12 – Time serie of 2-m temperature in Bromma Airport station between the 24th and the 27th of July, 2014, in USGS (red), MODIS(grey) and CORINE (green) simulations and observational data (black).

overestimates it during the night. The USGS simulation shows the lower daily maximum temperature while the MODIS and CORINE simulations show higher daily maximum values of temperature closer to the observational values. On the other hand, the USGS dataset shows also the lowest simulated daily minimum temperatures and it is the closest to the observations during the night.

3.2.2 Wind

Figure 13 shows the 10-m wind speed and direction field for the USGS simulations and the differences between this simulation and MODIS and CORINE simulations, on the 24th of July 2014 at 00:00 and at 12:00 UTC. As previously seen, the 24th July was included in the heat wave event, with very warm weather and relatively calm winds. At 00:00 UTC there was a week NNW flow with, maximum wind speed values of 5 m/s over the Baltic Sea and minimum values between 0 and 2 m/s over land. At 12:00 UTC it's possible to note an intensification of the wind speed and a clockwise rotation towards south.

This intensification of the windspeed is strongest in the region between the Swedish coast and Åland islands, and along the cost of Sweden, where it is possible to see the rotation from NNW in the night to ENE at 12:00 UTC, suggesting the occurrence of sea breeze. Besides this, also the vertical profiles for u and v wind components along the W-E cross-section showed in Figure 7, presented Annex 1 (Figure 26) shows the occurrence of this effect.

The windspeed differences between the model runs, MODIS and CORINE, and the control simulation USGS, show similar distributions, but different windspeed amplitudes. It is also possible to see that the differences, both in wind speed and direction, are largest at 12:00 than at 00:00 UTC and in MODIS simulation.

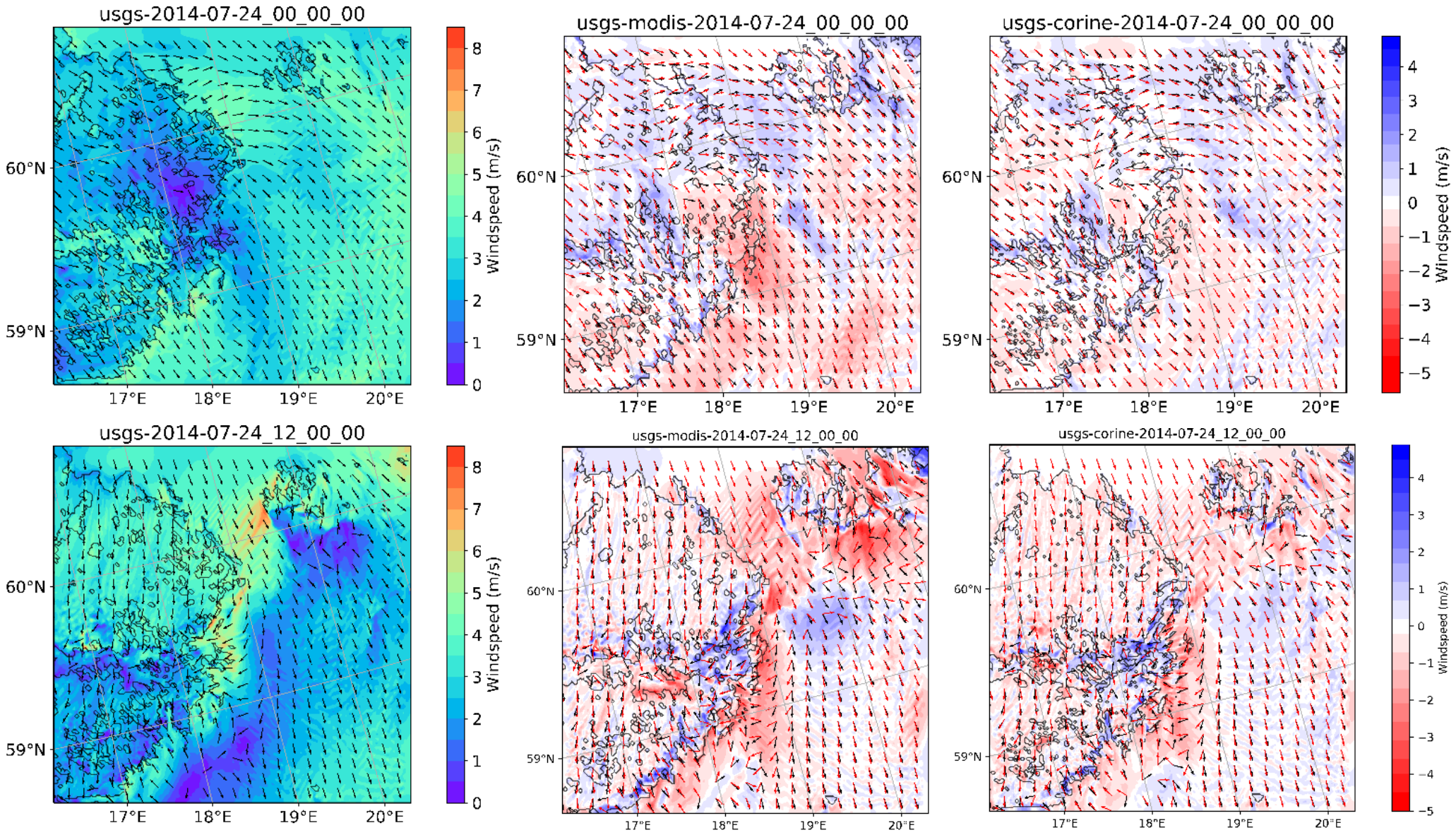

Figure 13 – 10-m wind speed spatial distribution for d03 in USGS (left), and diference between USGS and MODIS (center) and CORINE (rigth) simulations, on the 24th of July 2014, at 00:00 (top) and 12:00 (bottom).The black arrows represent the the USGS wind direction and the red arrows represent the MODIS and CORINE wind direction.

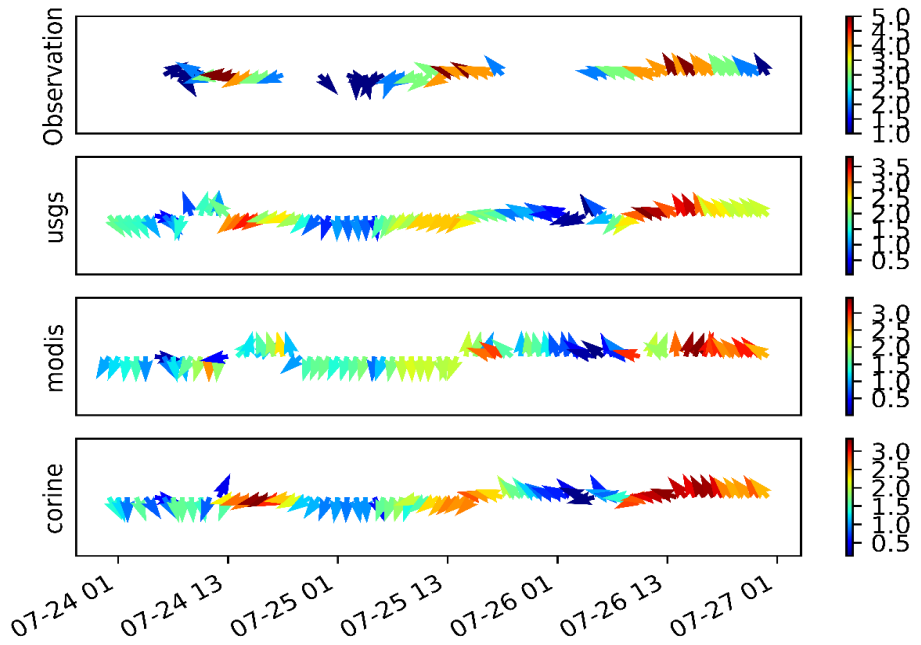

Figure 14 - Time series of 10-m wind speed in Bromma Airport station, and in USGS, MODIS and CORINE simulations, between the 24th and the 27th of July, 2014.

Figure 14 shows the observed and simulated hourly mean wind speed and direction evolution in Bromma Airport, during the three warmest days of the simulated period. It's possible to note that, during this period, the winds were usually calm during the morning, and showed an intensification during the afternoon, ranging between 1-5 m/s. When considering the timeseries from observations, USGS, MODIS and CORINE simulation, it is important to note the different color scales.

3.2.3 Validation

The results presented above showed that the use of different landuse datasets in the model simulations induce changes in the simulated temperature and wind speed fields. In order to assess the landuse dataset that produce the best results for the simulated period, the model simulations were compared against observation data. Figure 15 presents Taylor diagrams for all available data of 2-m temperature and u and v wind components. The Taylor diagram for 2-m temperature shows that CORINE and MODIS simulations present higher correlation and smaller RMSE values than USGS simulation, although MODIS performed slightly better as its Standard deviation is closer to the observed.

Analyzing the Taylor diagram for the u wind component, it is possible to note that the three simulations show similar correlation coefficients, although USGS's and CORINE's correlations are slightly higher than MODIS's. On the other hand, MODIS presents a Standard deviation closest to the observed and slightly lower RMSE.

The Taylor diagram for the v wind component shows that CORINE and USGS simulations present the best correlation with observed data, although lower than the

correlations for u component, and that USGS and MODIS present the standard deviation closer to the observations. USGS simulation showed the lower RMSE value when compared with the two other simulations performed in this test.

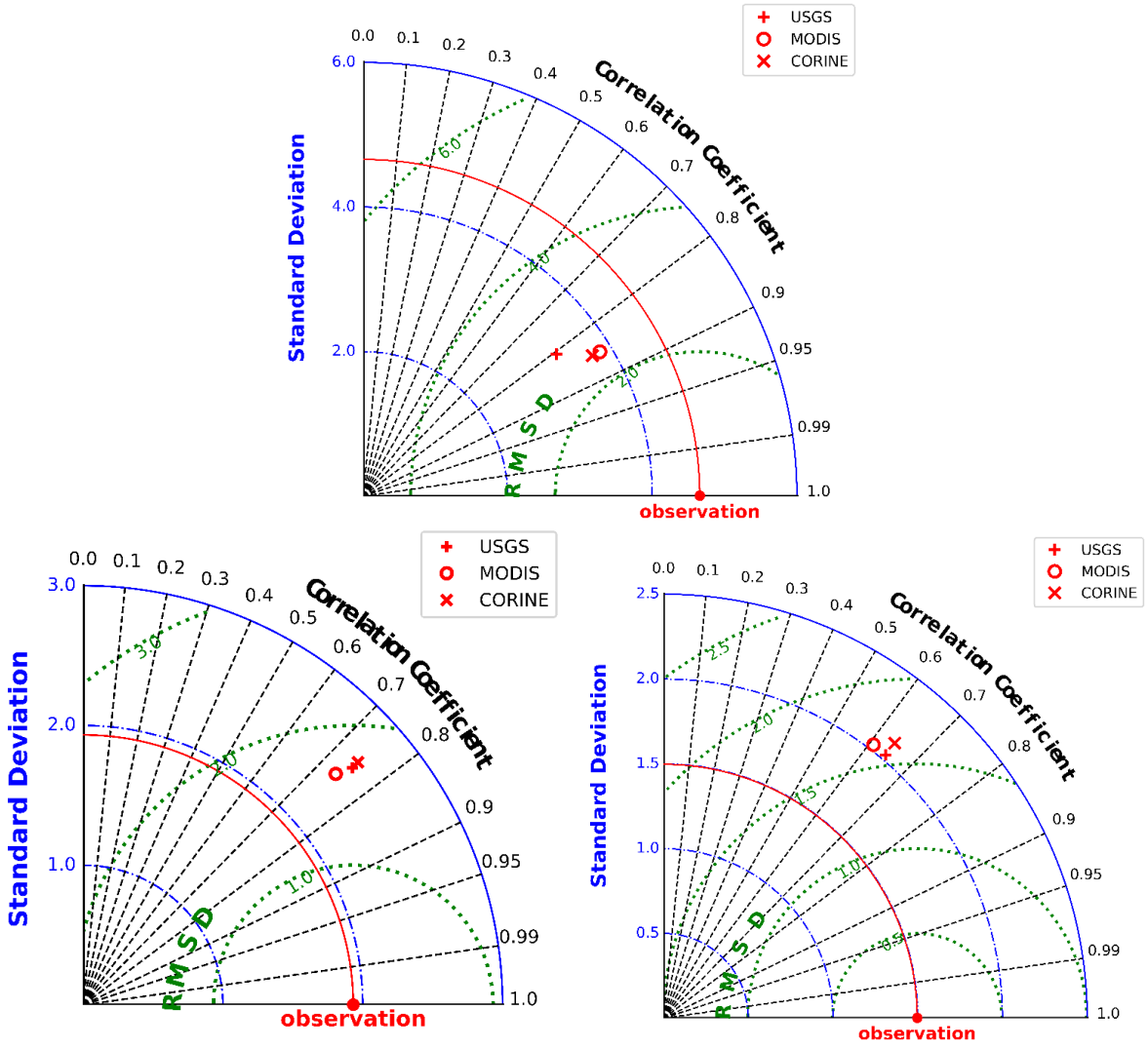

Figure 15 – Taylor diagram for 2-m temperature (a), 10-m wind U-component (b) and V-component (c) for all simulated period.

3.3 UCMs sensitivity test

In this section the results from the UCM's sensitivity tests are presented. As previously seen, in the UCMs sensitivity test, the CORINE landuse dataset was used in the three simulations performed, in order to take advantage of the three urban categories used by the UCM in the WRF model. The simulation without a UCM (CORINE), was used as a control run, and two simulations were performed using a UCM, the single layer UCM (SLUCM) and BEP model (BEP).

3.3.1 2-m Temperature

The 2-m temperature results for the control simulation and the differences between this simulation and SLUCM and BEP simulations, at 12:00 UTC during the 24th of July and the 8th of July are showed in Figure 16, in order to represent the differences between simulations during the heat wave event and after the event.

Positive and negative differences can be found for both simulations, with a similar spatial distribution between them, but, with small localized differences in amplitude, in both days, during and after the heat wave. It is possible to note that, in regions around urban areas, temperature differences are positive in both UCM and BEP simulations, showing a cooling effect introduced by the use of UCMs. This effect had been described by Teixeira (2012) for Lisbon region and it can be associated with the green area fraction considered by the models for each urban class. In CORINE simulation, the Noah Land Surface model considers a 10% of green fraction area for the Urban and Built-Up category, while this fraction correspond to 50% in UCMs, the urban grid-cells with Low density residential, which are the most represented urban class in the domain. It is also possible to note that these differences have a larger amplitude during the heat wave than afterword's, showing an intensification of the nocturnal UHI during the heatwave event.

3.3.2 Wind

Figure 17 shows the wind speed and direction for the control simulation and the differences between this simulation and UCM and BEP simulations, during the 24th of July and the 8th of July at 12:00 UTC. On the 24th July, it is possible to see the occurrence of calm, northerly winds, over land, with maximum values of 5 m/s, in the northern region of the domain, while in the coastal regions the flux is intensified, reaching 8 m/s and rotates clockwise towards the West. A zone of wind flow intensification is also possible to note between the Swedish coast and the finish Åland islands. The differences between UCMs simulations and the control, during the heatwave event, show that the UCMs generally increase the windspeed, particularly in coastal regions over the sea, and decrease it in the terrestrial coastal areas. During this event, the largest differences in the wind direction were found in zones of minimum wind speed values and in the coastal area over the sea.

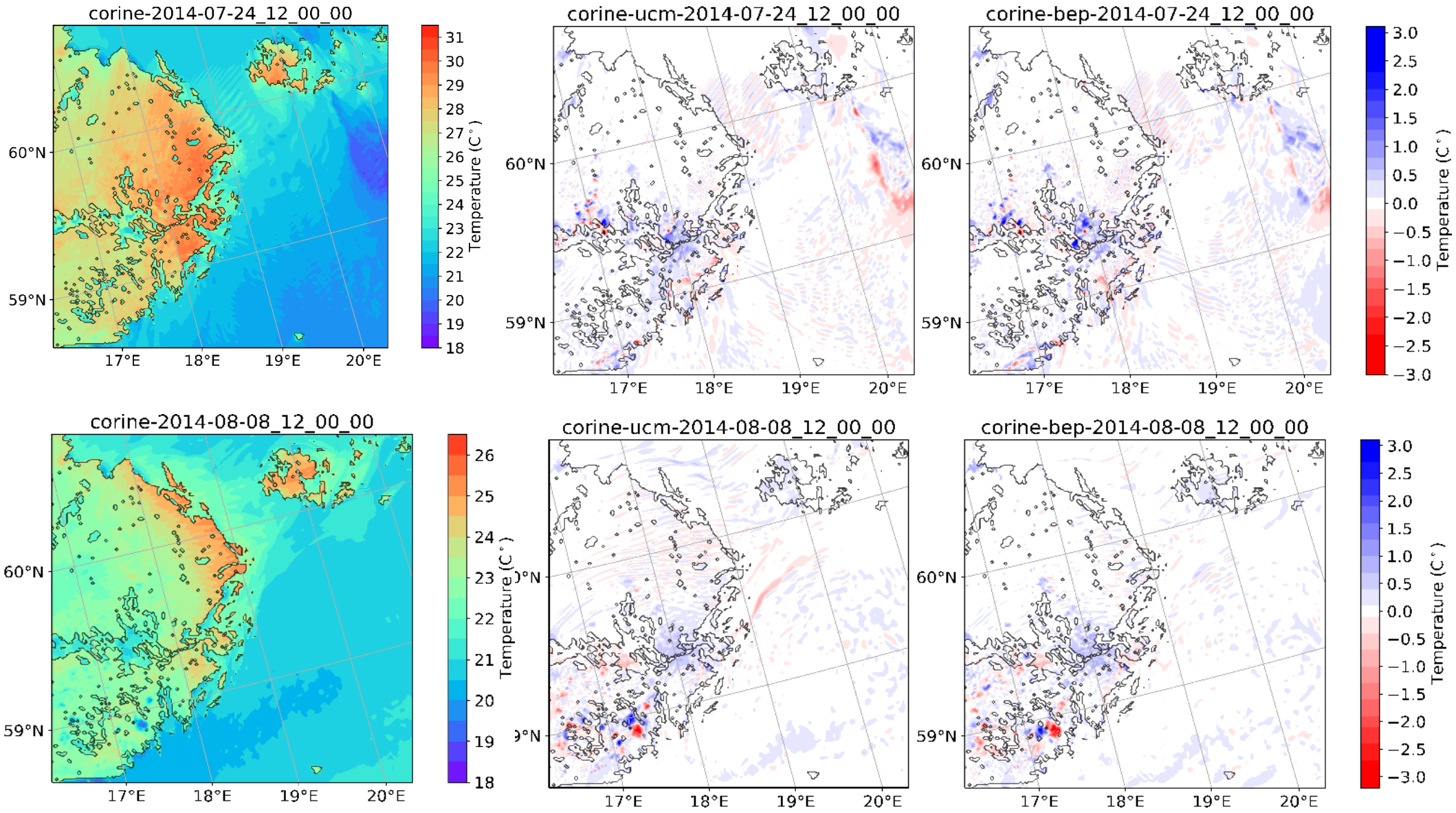

Figure 16 - 2 m temperature spatial distribution for d03 in the control simulation (left), and diference between the control and UCM (center) and BEP (rigth) simulations, on the 24th of July 2014, (top), and on the 8th of July 2014 (bottom), at 12:00 UTC.

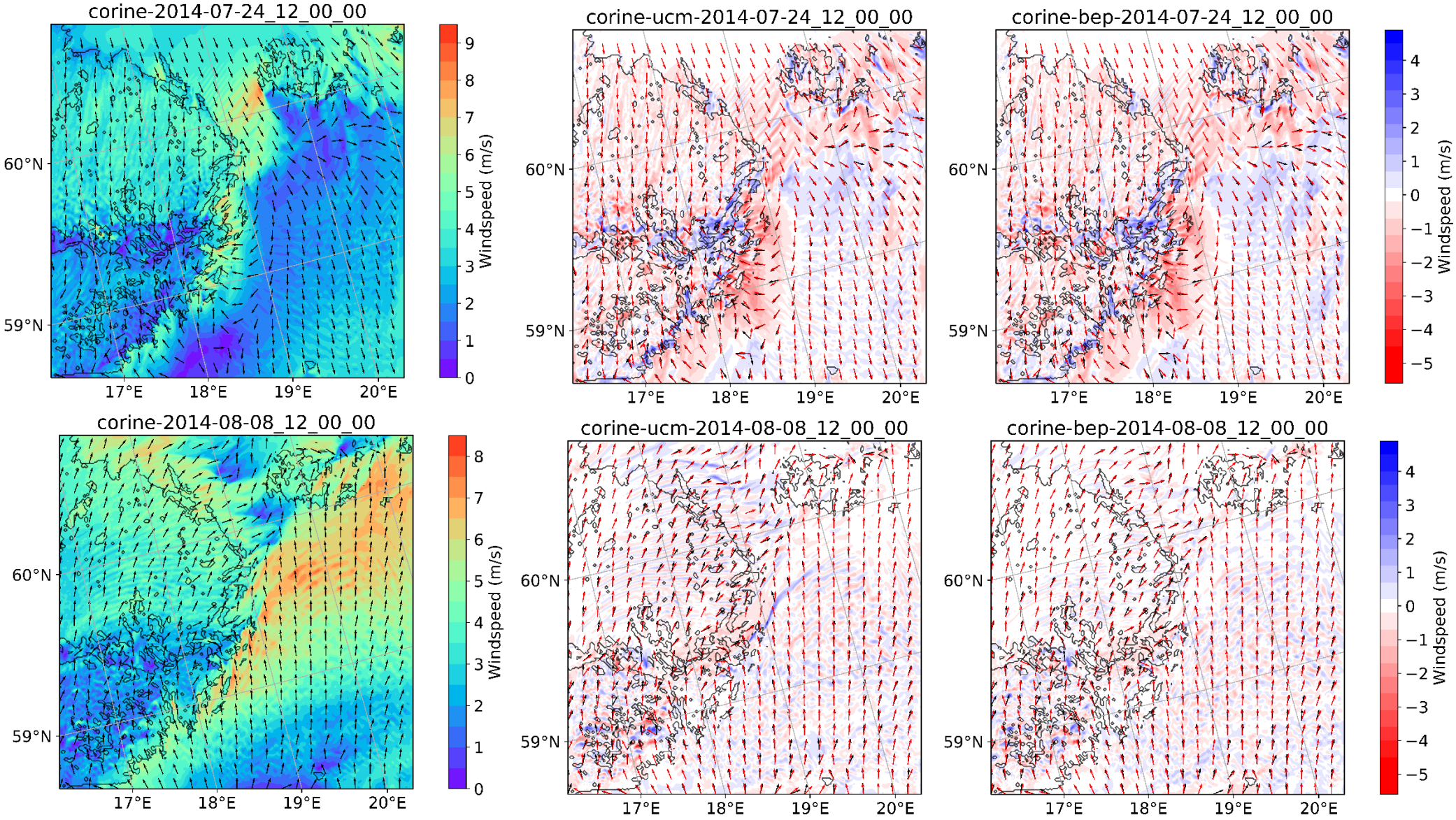

Figure 17 - 10 m windspeed and direction spatial distribution for d03 in the control simulation (left), and diference between CORINE and UCM (center) and BEP (rigth) simulations, on the 24th of July 2014, (top), and on the 8th of July 2014 (bottom), at 12:00 UTC.

The results for the control simulation on the 8th of August shows a southerly flow, with a wind speed between 0-5 m/s over land and stronger winds located over the Baltic sea, reaching 8 m/s. The windspeed differences between the UCMs and the control simulations were considerably smaller than the differences found during the heatwave event.

3.3.1 UHI effect

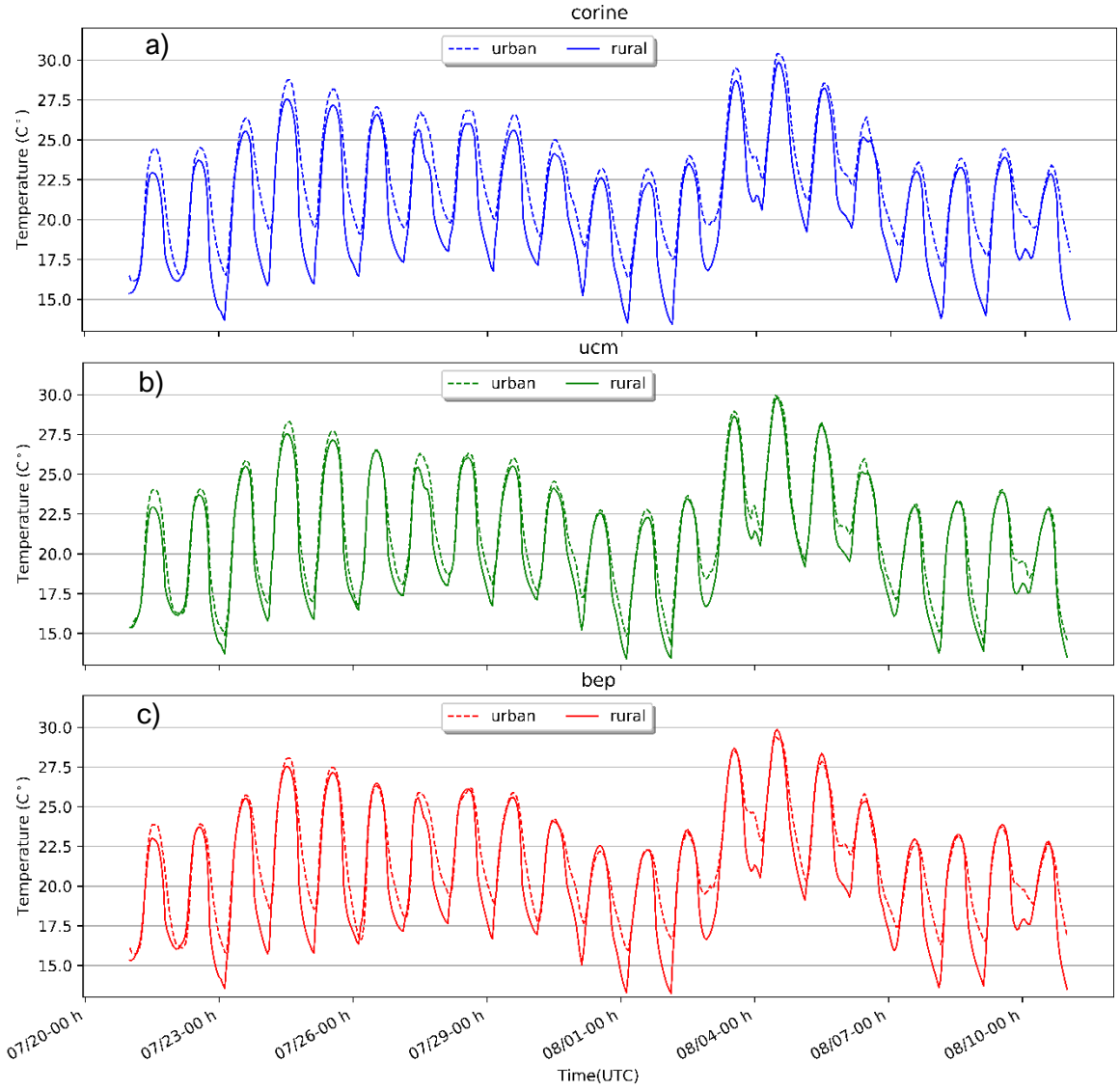

Figure 18 - Hourly time series for 2-m temperature of all rural and all urban grid cells in CORINE (a), UCM (b) and BEP (c) simulations, for all simulated period.

As previously seen, the UHI effect corresponds to the temperature difference between the urban and the surrounding rural area. In order to study the UCMs performance in simulating the UHI effect, the average temperature of all urban and non-urban grid points

was calculated. The three urban categories (High density residential, Low density residential and Commercial/Industrial/Transportation) were considered for urban categories, while for rural categories, all the non-urban grid-points except water bodies were considered.

The results of the rural and urban temperatures are showed in Figure 18, for CORINE, UCM and BEP simulations. It is possible to observe that the control simulation, produce the highest urban temperatures and larger differences between urban and rural areas, while the use of UCMs reduced considerably the temperature of urban areas, and therefore the differences between urban and rural temperatures. Also, the use of the single layer UCM produces a lower daily minimum urban temperature and, therefore, a smaller difference between the rural temperatures during the day.

To understand the performance of the different UCMs simulating the UHI effect, during a warm weather event, the results of urban and rural temperatures were compared for two sub-periods of three days, one between the 24th and the 27th July, included in the heat wave event affecting Scandinavia, and the other between the 8th and the 11th of August, that represents the sub-period with the lowest temperatures found during the entire simulated period.

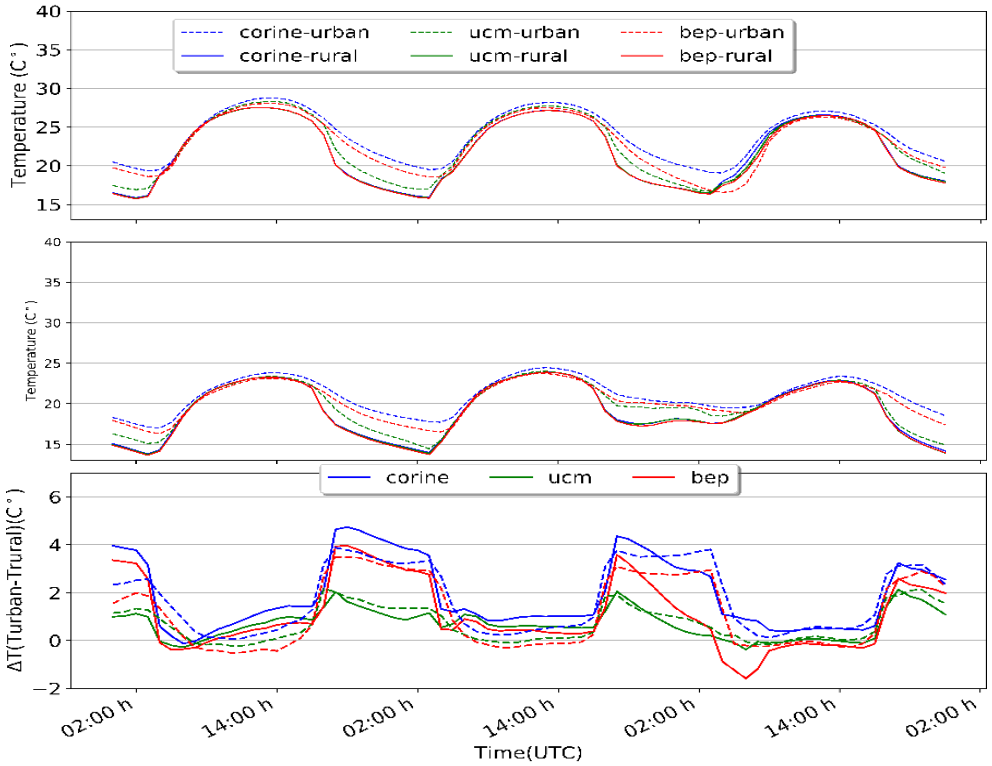

Figure 19 - Hourly averaged 2-m temperature of all rural and all urban grid cells in CORINE, UCM and BEP simulations, during the first sub-period, from 24 to 27 of July (top)during the second sub-period, from 7 to 10 of August , and the respective difference between all urban and all rural grid-points for all simulations (bottom), during the first sub-period (solid line) and the second sub-period (dashed line).

Figure 19 illustrates the urban and rural temperatures, and its difference, during these two sub-periods. It's possible to see that the introductions of a UCM induces significant changes simulating the urban temperature while differences in the rural temperature are very small. The results show that the maximum temperature difference between urban and rural temperatures usually occur during the evening and extends until the sun rise around 3:30 UTC; and that the minimum vales are usually found during the day, with differences around zero, or even rural temperatures exceeding the urban temperatures.

During both sub-periods analyzed, the control simulation, CORINE showed the maximum difference between urban and rural temperatures, with a maximum difference of 5ºC during the night of 24th July, simulating the larger UHI effect. The BEP simulation presented a maximum difference of 4ºC between urban and rural temperatures, while UCM simulated a maximum difference of 2ºC.

The comparison between the two sub-periods showed that maximum differences between urban and rural temperatures is higher during the first sub-period, during the first two days, in both CORINE and BEP simulations, suggesting an intensification of the nocturnal UHI with the increase in temperature. During the third day, the temperature difference between the two sub-periods is smaller producing a smaller difference in the UHI intensity between the two periods. It´s also possible to note that the single layer UCM produces the smaller differences between the two subperiods.

Figure 20 present a closer view of the 2-m temperature around Stockholm city from BEP simulation on the 24th July at 00:00 UTC and the respective landuse.

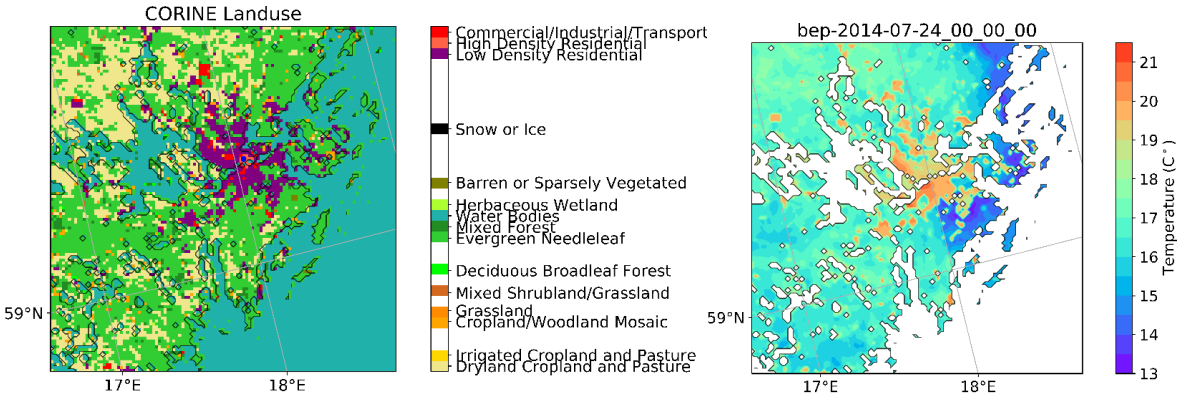

Figure 20 – CORINE landuse map (left) and 2-m temperature from BEP simulation on the 24th July at 00:00 UTC (right), on the Stockholm city region.

The previous results showed significant differences in the UHI intensity calculated with the UCMs. To understand which simulation represents best this effect, the model results of 2-m temperature were compared against observations. One simple method to calculate the UHI effect using data from meteorological stations, is measuring the temperature difference between the temperature in an urban station and in the surrounding

rural stations. Given this, the average temperature difference between Stockholm A station, and the remaining stations available in the domain ($\Delta T_{(Stockholm-station)}$), was calculated and compared with the simulations.

Table 6 shows the results for each station, and the mean results for all stations, calculated over the whole simulation period. Significant differences were found amongst the stations. The maximum difference was 1.96ºC, between Stockholm temperature and *Svanberga A*, and the minimum 0.68ºC in *Bromma* station, located in the city center less than 10 km from the *Stockholm* Station. The mean difference found between Stockholm temperature and the other stations was 1.38ºC, and the model that better represented this difference was the single layer UCM. The single layer UCM also performed better for a larger number of stations than the BEP or CORINE simulations.

Table 6 – $\Delta T_{(Stockholm-station)}$, calculated from observational data, CORINE, UCM and BEP simulations, for all simulation period. The best results are highlighted in grey.

	21/07/2014 - 11/08/2014			
	OBS	*CORINE*	*UCM*	*BEP*
Svanberga A	*1.96*	*1.11*	*0.28*	*0.23*
Berga Mo	*1.30*	*1.43*	*0.88*	*0.74*
Uppsala	*1.38*	*2.08*	*1.33*	*1.314*
Bromma	*0.68*	*-0.17*	*-0.13*	*-0.10*
Film A	*1.12*	*2.60*	*1.72*	*1.70*
Galve A	*1.53*	*1.25*	*1.55*	*0.79*
Tullinge A	*1.81*	*1.15*	*0.67*	*0.65*
Arlanda	*0.87*	*0.78*	*0.43*	*0.31*
Adelso	*1.14*	*2.06*	*1.19*	*1.31*
Eskilstuna A	*1.72*	*3.14*	*2.25*	*2.37*
Enkoping	*1.35*	*2.33*	*1.58*	*1.55*
Sala	*1.67*	*2.92*	*1.98*	*1.99*
Mean	*1.38*	*1.72*	*1.14*	*1.07*

Table 7 shows the temperature difference between Stockholm station and the other stations available in the domain, during the previous selected sub-periods namely, 24th to 27th of July and 8th to 11th of August. The results show that the CORINE simulation represent best the UHI effect intensification during the heat wave event, while the use of a UCM considerably underestimates the observed UHI. On the other hand, during the second sub-period the UHI effect is less intense, and the SLUCM showed the best results in simulating this effect.

Table 7 - $\Delta T_{(Stockholm\text{-}station)}$, calculated from observational data, CORINE, UCM and BEP simulations, for and the two sub-periods, between the 24th and the 27th of July between the 8th and the 11th of August, 2014. The best results are highlighted in grey.

	[24/07/2014 - 27/07/2014]				[08/08/2014 - 11/08/2014]			
	OBS	CORINE	UCM	BEP	OBS	CORINE	UCM	BEP
Svanberga A	3.86	2.25	1.28	0.93	1.66	0.90	0.07	0.07
Berga Mo	2.98	1.81	1.22	0.92	0.54	1.05	0.37	0.58
Uppsala	2.67	2.28	1.28	0.76	0.91	2.27	1.307	1.45
Bromma	1.23	-0.33	-0.23	-0.13	0.63	0.04	0.01	0.02
Film A	2.14	3.01	2.00	1.58	1.07	2.85	1.90	1.93
Galve A	3.47	1.12	1.48	0.30	0.83	0.88	0.78	0.38
Tullinge A	3.19	1.17	0.59	0.43	1.61	1.43	0.91	0.91
Arlanda	1.27	0.79	0.39	-0.00	0.68	0.76	0.36	0.27
Adelso	2.44	2.36	1.34	1.14	0.70	2.21	1.23	1.54
Eskilstuna A	2.92	2.71	1.71	1.47	1.42	3.07	2.12	2.29
Enkoping	2.06	2.24	1.32	0.93	1.07	2.53	1.87	1.60
Sala	2.43	2.16	1.16	0.72	1.06	2.91	1.89	2.03
Mean	2.56	1.80	1.13	0.75	1.02	1.74	1.07	1.9

Table 8 - ΔT (Stockholm-station), calculated from observational data, CORINE, UCM and BEP simulations, for and the two sub-periods, between the 24th and the 27th of July between the 8th and the 11th of August, 2014, between 20:00 and 03:00 UTC. The best results are highlighted in grey.

	[24/07/2014 - 27/07/2014]				[07/08/2014 - 10/08/2014]			
	OBS	CORINE	UCM	BEP	OBS	CORINE	UCM	BEP
Svanberga A	8.05	4.58	3.02	2.57	3.66	1.95	0.93	1.07
Berga Mo	4.454	1.75	0.60	-0.08	1.24	1.35	0.26	0.64
Uppsala	5.97	3.80	2.26	1.54	2.08	4.00	2.59	3.07
Bromma	3.34	-0.48	-0.20	-0.10	1.71	0.09	0.06	0.08
Film A	5.13	5.30	3.51	2.82	2.94	5.49	4.14	4.38
Galve A	6.73	0.66	2.07	-0.75	2.46	2.04	1.95	1.10
Tullinge A	7.13	1.72	0.65	0.11	3.14	2.04	0.99	1.09
Arlanda	3.18	1.34	0.42	-0.18	1.38	1.01	0.36	0.22
Adelso	5.90	3.56	1.79	1.33	2.30	3.37	1.93	2.71
Eskilstuna A	6.30	4.24	2.44	1.79	4.24	4.69	3.55	3.88
Enkoping	4.96	3.54	1.96	1.40	2.93	4.03	3.09	2.99
Sala	5.41	3.44	1.80	1.04	2.97	4.89	3.37	3.72
Mean	5.55	2.79	1.69	0.96	2.59	2.91	1.93	2.08

Additionally, the model performance calculating the UHI effect was studied during the night, in order to access the best model performing the nocturnal UHI effect. Table 5 shows the temperature difference between Stockholm station and the other stations, for the two selected sub-periods, between 20:00 and 3:00 UTC. The results show an increase of the UHI effect during the night both sub-periods considered. During the heatwave event, the mean difference between Stockholm A station and the other stations during the night was 5.55ºC, while during the second sub-period it was 2.59ºC. The model results show that UCMs underestimate the UHI effect; and CORINE simulation, which produces higher urban temperatures, show a better performance simulating this effect.

3.3.2 Vertical Structure

The PBL height from CORINE simulation and the difference between this and UCM and BEP simulation are presented in Figure 21 for the 24th of July and the 8th of August 2014. It is possible to observe that, on the 24th July, the maximum PBL height is higher than during the 8th August, as observed in the 2-m temperature results, although in both days, one can notice some spots over land, with an abrupt reduction of PBL height. Positive and negative localized differences between the two simulations and the control were found in the domain, some with differences of 1500 m, corresponding to differences in the location of the zones with an abrupt reduction of the PBL height induced by the UCMs.

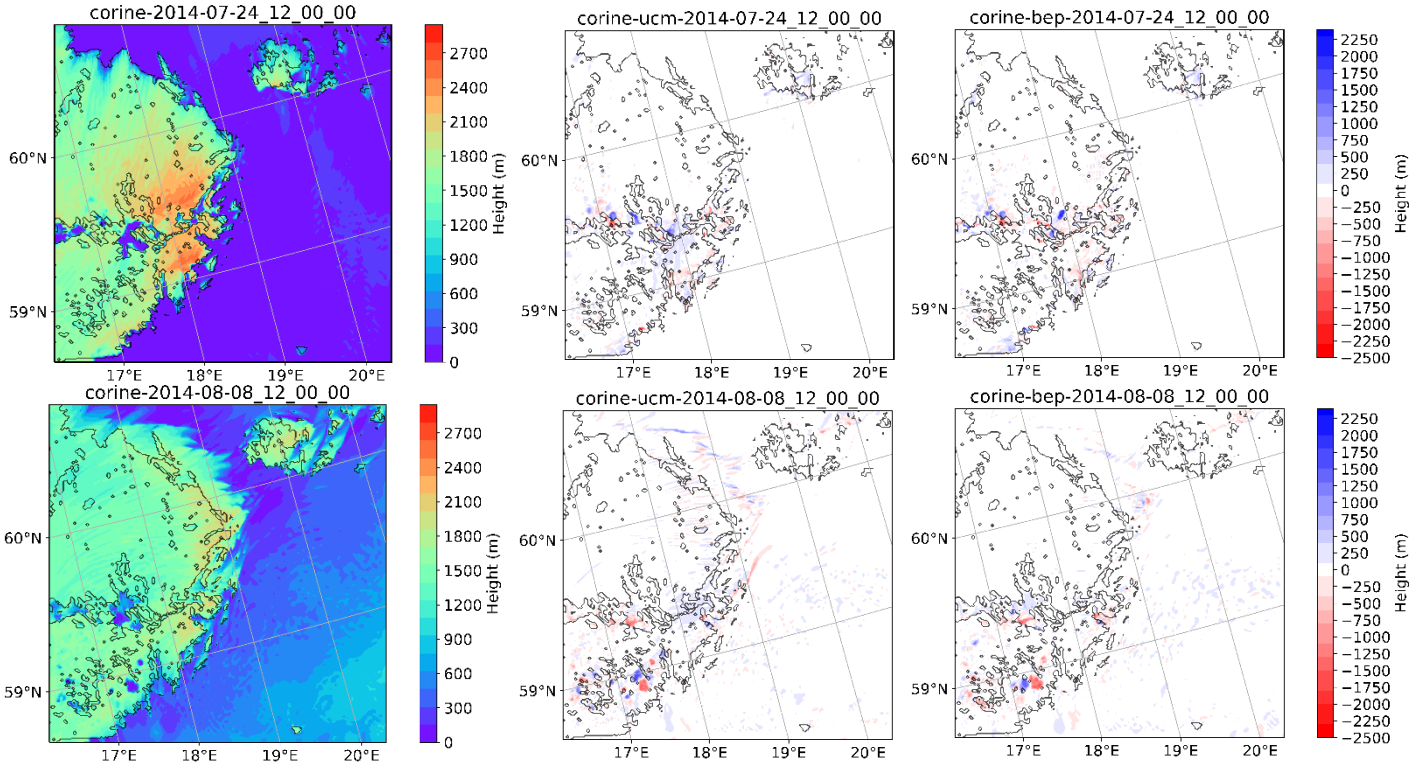

Figure 21 – PBL height (m) for CORINE simulation (left) and differences between CORINE simulation and UCM (center), and BEP (right) simulations, on the 24th July (top) and the 8th August (bottom) at 12:00 UTC.

The PBL height in urban regions is significantly higher than in the surrounding rural areas. Figure 22 shows the PBL height variation, for CORINE, UCM and BEP simulations, on different locations, two urban locations, *Stockholm A* and *Bromma* station, and two rural stations, *Svanberga A* and *Film A*, during the 24th July and the 8th of August 2014.

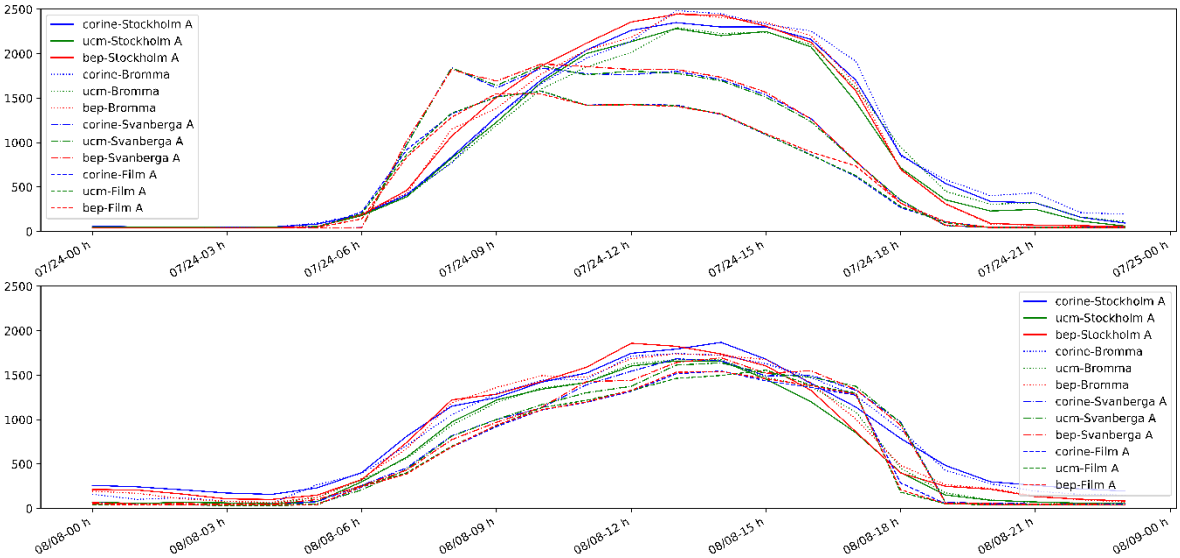

Figure 22 – Time series with the PBL height (m) from CORINE, UCM and BEP simulations, for Stockholm A. Bromma, Svanberga A, and Film A stations, during the 24th Jully (top) and 8th August (bottom).

It is possible to note that the PBL height is higher on the 24th than on the 8th August. The results show that the PBL height in urban locations, *Sotckholm* and *Bromma* are quite similar as they are separated by a small distance, while the rural locations present lower PBL heights. It is also possible to note that the difference between rural and urban PBL heights is larger on the 24th July than the 8th August. During the first day, BEP simulation calculates the UBL height, at *Stockholm A* station more than 700 m above the PBL height at *Svenberga A* location, while during the 8th August the maximum difference was less than 400 m, and only lasted for a couple of hours.

As previously seen, the urbanized regions can significantly modify the PBL proprieties over large cities, forming the so called UBL. In order to study the model sensitivity to UCMs, calculating the vertical structure of the atmosphere, the wind flow, potential temperature and turbulent kinetic energy (TKE) vertical structures were analyzed along a N-S cross-section, centered over Stockholm city center station (represented in Figure 7). Figure 23 shows the TKE and potential temperature, for CORINE simulation, and the difference between these and the UCM and BEP model, during the heatwave event, on the 24th July at 12:00 UTC. The TKE is directly related with the transport of momentum, heat and moisture, trough the boundary layer. It's possible to see that large values of TKE occur within the firsts thousand meters above the land surface, with maximum values occurring between Stockholm and the coastline. Over the Baltic sea and other water bodies within the

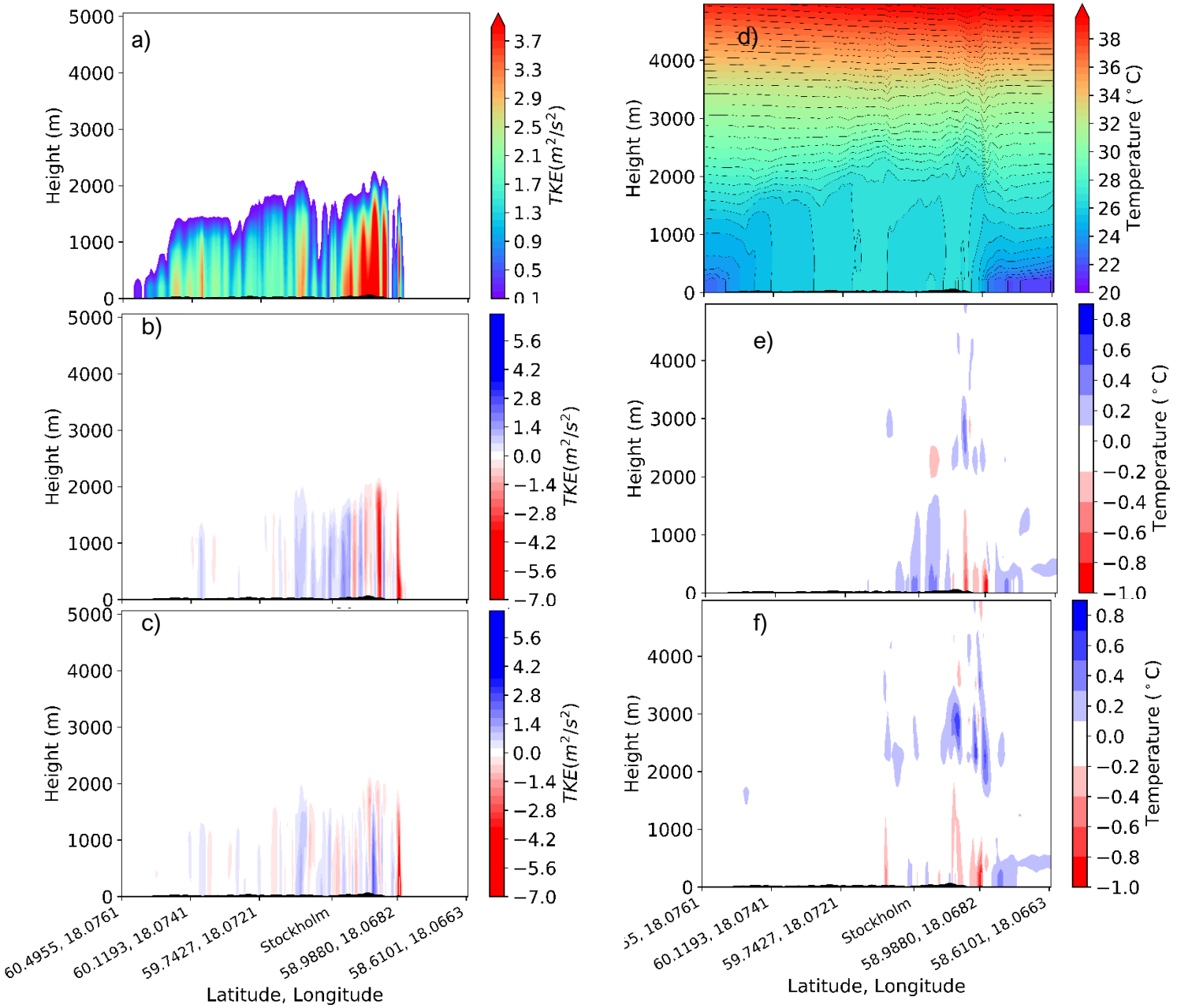

Figure 23 – Vertical cross section for the Turbulence Kinetic Energy (TKE) (a) and for Potential Temperature (d), in CORINE simulation (a) and difference between UCM b) and e) and BEP c) and f) at 24th July 12:00 UTC.

domain, the TKE is close to zero, showing no vertical mixing, caused by the high stability present in these zones. The comparison between the UCMs simulation and the control shows that the SLUCM simulation presents lower values of TKE over Stockholm location, but higher values over urban areas, than the control. On the other hand, BEP simulation shows smaller differences from the control simulation.

The potential temperature cross section shows a zone of constant potential temperature between the surface and 2000m, highlighting a well-mixed layer over these regions. It's also possible to note that above rural regions, the mixed layer is thinner than over urban areas and that over the sea, the mixed layer is even smaller due to strong

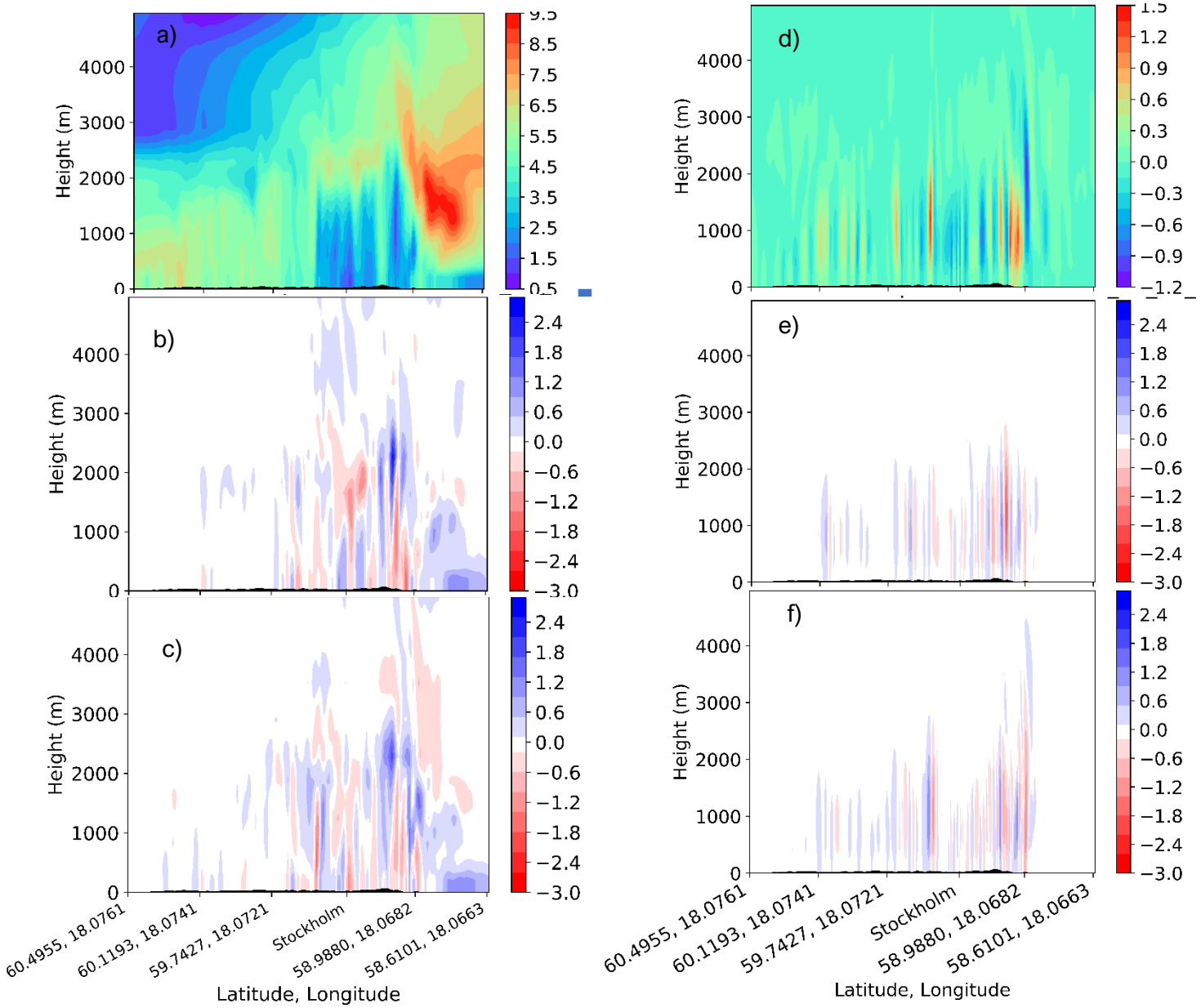

Figure 24 - Vertical cross section for windspeed (a) and w vertical wind-component(d) from CORINE simulation, and the differences between CORINE simulation and UCM b) and e), and BEP simulations c) and f), on the 24th July 12:00 UTC.

stability. The differences between the UCMs simulations and the control shows that the SLUCM produces lowest potential temperature values around 58.988 ºN and highest values north and south from this area. The BEP simulation on the other hand, shows higher potential temperatures around 58.988 N than the control simulation. Both UCMs simulations present lower values of potential temperature above the UBL than the control simulations, although differences in BEP simulation are greater than in the SLUCM simulation, showing that changes induced by BEP model have a stronger impact reducing the potential temperature of upper levels of the atmosphere.

Figure 24 show the vertical cross sections of wind speed and vertical wind component-w during the 24th July at 12:00 UTC, for the CORINE simulation, as well as the differences between this simulation and SLUCM and BEP. The wind-speed cross section from the control simulation shows that the wind speed is significantly smaller in the urban areas around Stockholm, when compared to the region further north. It is also possible to note a wind speed maximum at 500 m height over the coastal region. The differences between the UCMs simulation and the control simulation showed that the introduction of these models modifies the structure of the windspeed in the PBL, and on upper atmospheric levels of urban regions. Besides this, the SLUCM produced larger differences from the control simulations, than BEP.

The results for the vertical motion cross section of the control simulation showed both positive and negative vertical motion over land, between -1.2 and 1.5 m/s, mostly within the first two km of the atmosphere, showing the vertical mixing of the PBL caused by the warming of the surface. It is also possible to note that the introduction of the UCMs can change the vertical wind motion components by 3 m/s in localized regions located around urban regions, within the first 2 km in SLUCM and 4 km in BEP simulation.

3.3.3 Validation

The previous results showed significant differences in temperature and wind fields between the simulations. To evaluate the model performance, the modeled data was compared against observations. The results for the simulated 2-m temperature and 10-m wind components (u and v) are showed in the Taylor diagrams of Figure 25. For temperature, it is clear that the model performs well, with very small differences between the three simulations, with correlation coefficients around 0.85, RMSD close to 2.5 and the standard deviation close to the observed. Nevertheless, SLUCM simulation shows a better performance as it presents a slightly higher correlation coefficient, lower RMSE and the standard deviation is closest to the observed. Regarding the wind components diagrams, it results for the two components are very similar, although the u component shows higher correlations coefficients and lower RMSE than the v component. Despite this, BEP simulation has the best performance for both wind components, as it presents a standard deviation closer to the observed, a slightly lower RMSE and higher correlations values.

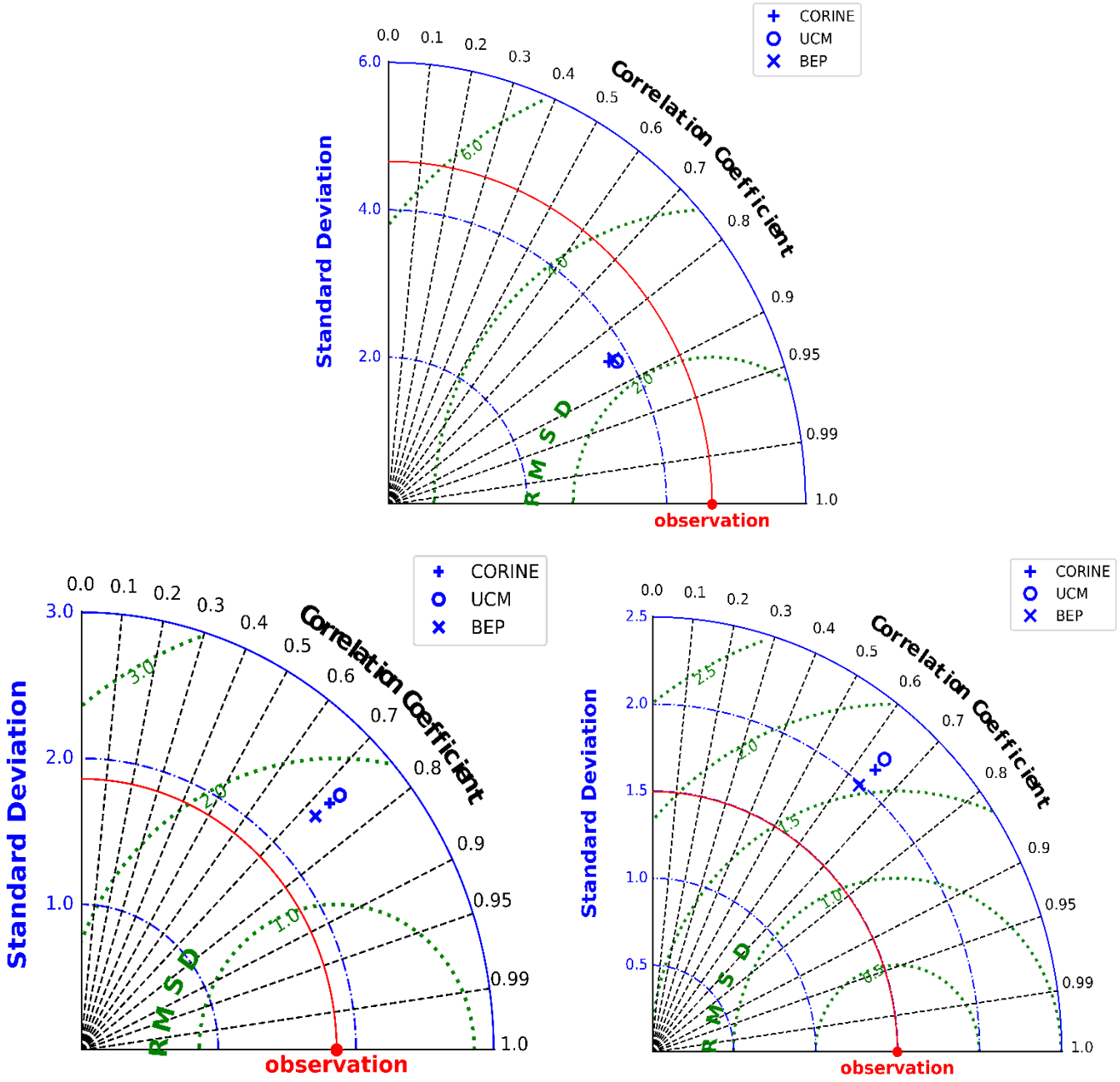

Figure 25 - Taylor diagrams for 2-m temperature (a), 10-m wind U-component (b) and V-component (c) for all simulated period.

4 Conclusions

Heatwaves are among the most dangerous extreme weather events, posing a significant threat to environment and society and their occurrence are projected to significantly increase over Europe in a climate change scenario. Densely urbanized regions as cities, are more vulnerable to extreme hot weather events, than rural areas, due to pre-existing UHI effect. The present work evaluates the WRF model sensitivity to landuse and UCM parametrizations, during a heat wave event occurring in Stockholm region. This study was focus on a period of unusual hot weather, occurring in July and August 2014, where a strong influence of a high-pressure system favored strong surface heat, and calm winds, leading to several heat related alarms from the Swedish authorities.

First, the WRF model was tested with three different landuse datasets, the model default and older dataset, USGS, MODIS, with the same resolution of USGS but more recent, and CORINE, with a higher resolution than the previous datasets. The larger differences between simulations were found mostly where the landuse is also different, for instance where one represents water and the other land. This reveled to be especially important in the studied domain, characterized by a very irregular coastline and the presence of many little islands and lakes. Temperature and wind differences showed that the landuse parameters used by the model has a larger impact in the simulations than the use of a high-resolution dataset, as MODIS showed bigger differences with the USGS simulations than CORINE that uses the same parameters than USGS.

When comparing the model results with observations, it was found that using a high-resolution or more updated landuse dataset, as CORINE and MODIS, improves the model performance simulating the 2-m temperature and wind u-component field.

The second test performed in this study, investigates the WRF model sensitivity to the coupling of to UCMs, the SLUCM and the BEP model, using a high resolution landuse dataset, namely CORINE. The results showed that the performances obtained with the UCMs strongly depend on the landuse parameters representing the city. The cooling effect found in densely urbanized regions produced by SLUCM and BEP simulations is an example of how the green fraction parameter influences the surface temperature in urban regions. Furthermore, it was observed that this cooling effect is stronger in the presence of higher temperatures.

The 2-m temperature results showed that the UHI effect occurs during the simulated period, and that this effect is stronger during the night and during warmer days. The SLUCM simulation showed a better performance representing the UHI effect, during all the simulation period. However, during the heatwave event CORINE simulation performed better. The results showed that adding a UCM to the model simulation, produces significant

differences in wind speed and direction, where BEP showed the best performance, but very small differences in the simulation of the 2-m temperature, although SLUCM showed a slightly better performance.

The results obtained in this work were found to be strongly the dependent on the parameters that describe landuse proprieties and characteristics of the city. New studies should be performed using specified parameters adequate to characterize the city in study.

5 References

Bougeault, P. and Lacarrère, P. (1989) Parameterization of Orography-Induced Turbulence in a Mesobeta-Scale Model. Monthly Weather Review, 117, 1872-1890.

Chen, F., and J. Dudhia, 2001: Coupling an advanced land-surface/ hydrology model with the Penn State/ NCAR MM5 modeling system. Part I: Model description and implementation. Mon. Wea. Rev., 129, 569–585.

Cheng, F., Hsu, Y., Lin, P., & Lin, T. (2013). Investigation of the Effects of Different Land Use and Land Cover Patterns on Mesoscale Meteorological Simulations in the Taiwan Area. Journal Of Applied Meteorology And Climatology, 52(3), 570-587. doi: 10.1175/jamc-d-12-0109.1

Dudhia, J., 1989: Numerical study of convection observed during the winter monsoon experiment using a mesoscale two-dimensional model, J. Atmos. Sci., 46, 3077–3107.

European Centre for Medium-range Weather Forecast (ECMWF) (2011): The ERA-Interim reanalysis dataset, Copernicus Climate Change Service (C3S) (accessed 19/03/2018), available from https://www.ecmwf.int/en/forecasts/datasets/archive-datasets/reanalysis-datasets/era-interim.

Fekih, A. and Mohamed, A. (2017). Evaluation of the wrf model on simulating the verticalstructure and diurnal cycle of the atmospheric boundary layer over bordj badji mukhtar (southwestern algeria). Journal of King Saud University-Science.

Grumm, R. (2011). The Central European and Russian Heat Event of July–August 2010. Bulletin Of The American Meteorological Society, 92(10), 1285-1296. doi: 10.1175/2011bams3174.1

Haylock, M.R., N. Hofstra, A.M.G. Klein Tank, E.J. Klok, P.D. Jones and M. New. 2008: A European daily high-resolution gridded dataset of surface temperature and precipitation. J. Geophys. Res (Atmospheres), 113, D20119, doi:10.1029/2008JD10201.

He, X., Li, Y., Wang, X., Chen, L., Yu, B., Zhang, Y., & Miao, S. (2019). High-resolution dataset of urban canopy parameters for Beijing and its application to the integrated WRF/Urban modelling system. Journal of Cleaner Production, 208, 373–383. https://doi.org/10.1016/j.jclepro.2018.10.086

Hofstra, N., Haylock, M., New, M., & Jones, P. D. (2009). Testing E-OBS European high-resolution gridded data set of daily precipitation and surface temperature. Journal of Geophysical Research, 114(D21). https://doi.org/10.1029/2009jd011799.

Hong, S.-Y., and J.-O. J. Lim, 2006: The WRF Single-Moment 6-Class Microphysics Scheme (WSM6), J. Korean Meteor. Soc., 42, 129–151.

IPCC, 2014: Climate Change 2014: Synthesis Report. Contribution of Working Groups I, II and III to the Fifth Assessment Report of the Intergovernmental Panel on Climate Change [Core Writing Team, R.K. Pachauri and L.A. Meyer (eds.)]. IPCC, Geneva, Switzerland, 151 pp.

Kain, J. S., 2004: The Kain-Fritsch convective parameterization: An update. J. Appl. Meteor.,43, 170–181.

Kim, Y., Sartelet, K., Raut, J., & Chazette, P. (2013). Evaluation of the Weather Research and Forecast/Urban Model Over Greater Paris. Boundary-Layer Meteorology, 149(1), 105-132. doi: 10.1007/s10546-013-9838-6

Kusaka, H., & Kimura, F. (2004). Coupling a Single-Layer Urban Canopy Model with a Simple Atmospheric Model: Impact on Urban Heat Island Simulation for an Idealized Case. Journal Of The Meteorological Society Of Japan, 82(1), 67-80. doi: 10.2151/jmsj.82.67

Kusaka, H., Kondo, H., Kikegawa, Y., & Kimura, F. (2001). A Simple Single-Layer Urban Canopy Model For Atmospheric Models: Comparison With Multi-Layer And Slab Models. Boundary-Layer Meteorology, 101(3), 329-358. doi: 10.1023/a:1019207923078

Kyselý, J., & Plavcová, E. (2010). A critical remark on the applicability of E-OBS European gridded temperature data set for validating control climate simulations. Journal of Geophysical Research, 115(D23). https://doi.org/10.1029/2010jd014123.

Li, D., & Bou-Zeid, E. (2013). Synergistic Interactions between Urban Heat Islands and Heat Waves: The Impact in Cities Is Larger than the Sum of Its Parts*. Journal of Applied Meteorology and Climatology, 52(9), 2051–2064. https://doi.org/10.1175/jamc-d-13-02.1

Lin, C.-Y., Chen, F., Huang, J. C., Chen, W.-C., Liou, Y.-A., Chen, W.-N., & Liu, S.-C. (2008). Urban heat island effect and its impact on boundary layer development and land–sea circulation over northern Taiwan. Atmospheric Environment, 42(22), 5635–5649. https://doi.org/10.1016/j.atmosenv.2008.03.015

Lopez-Espinoza, E.D., Zavala-Hidalgo, J., Gomez-Ramos, O., 2012. Weather forecast sensitivity to changes in urban land covers using the WRF model for central Mexico. Atmosfera 25, 127–154

Loridan, T., Grimmond, C., Grossman-Clarke, S., Chen, F., Tewari, M., & Manning, K. et al. (2010). Trade-offs and responsiveness of the single-layer urban canopy parametrization in WRF: An offline evaluation using the MOSCEM optimization algorithm and field observations. Quarterly Journal Of The Royal Meteorological Society, 136(649), 997-1019. doi: 10.1002/qj.614

Malakooti, H. (2010). Meteorology and air-quality in a mega-city: application to Tehran, Iran (Ph.D). École des Ponts ParisTech / Universite Paris Est.

Martilli, A., Clappier, A., & Rotach, M. (2002). An Urban Surface Exchange Parameterisation for Mesoscale Models. Boundary-Layer Meteorology, 104(2), 261-304. doi: 10.1023/a:1016099921195

Meehl, G. A., and C. Tebaldi, 2004: More intense, more frequent and longer lasting heat waves in the 21st century. Science, 305, 994-997, doi:10.1126/science.1098704.

Mlawer, E. J., S. J. Taubman, P. D. Brown, M. J. Iacono, and S. A. Clough, 1997: Radiative transfer for inhomogeneous atmosphere: RRTM, a validated correlated-k model for the longwave. J. Geophys. Res., 102 (D14), 16663–16682.

Oke, T. R., Mills, G., Christen, A., & Voogt, J. A. (2017). Urban Climates. Cambridge University Press. https://doi.org/10.1017/9781139016476

Osborn, A. (2010). Moscow smog and nationwide heat wave claim thousands of lives. BMJ, 341(aug10 2), c4360-c4360. doi: 10.1136/bmj.c4360

Perkins, S., & Alexander, L. (2013). On the Measurement of Heat Waves. Journal Of Climate, 26(13), 4500-4517. doi: 10.1175/jcli-d-12-00383.1

Perkins, S. E., Alexander, L. V., & Nairn, J. R. (2012). Increasing frequency, intensity and duration of observed global heatwaves and warm spells. Geophysical Research Letters, 39(20). https://doi.org/10.1029/2012gl053361

Pineda, N., Jorba, O., Jorge, J., & Baldasano, J. (2004). Using NOAA AVHRR and SPOT VGT data to estimate surface parameters: application to a mesoscale meteorological model. International Journal Of Remote Sensing, 25(1), 129-143. doi: 10.1080/0143116031000115201

Robine, J., Cheung, S., Le Roy, S., Van Oyen, H., Griffiths, C., Michel, J., & Herrmann, F. (2008). Death toll exceeded 70,000 in Europe during the summer of 2003. Comptes Rendus Biologies, 331(2), 171-178. doi: 10.1016/j.crvi.2007.12.001

Robinson, P. (2001). On the Definition of a Heat Wave. Journal Of Applied Meteorology, 40(4), 762-775. doi: 10.1175/1520-0450(2001)040<0762:otdoah>2.0.co;2

Salamanca, F., Martilli, A., Tewari, M., & Chen, F. (2011). A Study of the Urban Boundary Layer Using Different Urban Parameterizations and High-Resolution Urban Canopy Parameters with WRF. Journal Of Applied Meteorology And Climatology, 50(5), 1107-1128. doi: 10.1175/2010jamc2538.1

S.Rivera, M. (2018), Fog simulation on the north coast of Portugal. Retrieved from

http://hdl.handle.net/10773/25195.

Stull, R. B. (Ed.). (1988). An Introduction to Boundary Layer Meteorology. https://doi.org/10.1007/978-94-009-3027-8

Skamarock, W., Klemp, J., Dudhia, J., Gill, D., Barker, D., Wang, W., … Duda, M. (2008). A Description of the Advanced Research WRF Version 3. UCAR/NCAR. https://doi.org/10.5065/d68s4mvh

SMHI. Året 2014 - Rekordhög Sverigemedeltemperatur. Retrieved from https://www.smhi.se/klimat/2.1199/aret-2014-rekordhog-sverigemedeltemperatur-1.85064

Teixeira, J. (2012), WRF sensitivity to lower boundary and urban canopy parametrizations. Retrieved from http://hdl.handle.net/10773/10175.

Trigo, R. (2005). How exceptional was the early August 2003 heatwave in France?. Geophysical Research Letters, 32(10). doi: 10.1029/2005gl022410

United Nations, Department of Economic and Social Affairs, Population Division (2018). World Urbanization Prospects: The 2018 Revision, custom data acquired via website.

UrbanSIS – Climate Information for European Cities. (2019). Retrieved from http://urbansis.climate.copernicus.eu/

Wallace, J. M., & Peter Victor Hobbs. (2006). Atmospheric science: an introductory survey. Burlington, Ma: Elsevier Academic Press.

Wang, W., Bruyere, C., Duda, M., Dudhia, J., Gill, D., Lin, H. C., Michaelakes, J., Rizvi, S.,and Zhang, X. (2017). User's Guide for the Advanced Research WRF (ARW) Modeling System Version 3.9. Mesoscale & Microscale Meteorology Division.

Wilks, D. (2011). Statistical methods in the atmospheric sciences. Amsterdam: Elsevier/Academic Press.

Zhang, H., Jin, M., & Leach, M. (2017). A Study of the Oklahoma City Urban Heat Island Effect Using a WRF/Single-Layer Urban Canopy Model, a Joint Urban 2003 Field Campaign, and MODIS Satellite Observations. Climate, 5(3), 72. doi: 10.3390/cli5030072

Annex 1

Table 9 – USGS landuse categories and their physical parameters for 'summer' season taken from LANDUSE.TBL. Parameters from left to right are: Albedo (ALBD), soil moisture availability (SLMO), surface emissivity (SFEM), roughness length (SFZ0), thermal inertia (THERIN) and surface heat capacity (SFHC).

ALBD	SLMO	SFEM	SFZ0	THERIN	SFHC	Category
15.00	0.10	0.88	80.00	3.00	1.89E+06	'Urban and Built-Up Land'
17.00	0.30	0.99	15.00	4.00	2.50E+06	'Dryland Cropland and Pasture'
18.00	0.50	0.99	10.00	4.00	2.50E+06	'Irrigated Cropland and Pasture'
18.00	0.25	0.99	15.00	4.00	2.50E+06	'Mixed Dryland/Irrigated Cropland and Pasture'
18.00	0.25	0.98	14.00	4.00	2.50E+06	'Cropland/Grassland Mosaic'
16.00	0.35	0.99	20.00	4.00	2.50E+06	'Cropland/Woodland Mosaic'
19.00	0.15	0.96	12.00	3.00	2.08E+06	'Grassland'
22.00	0.10	0.93	5.00	3.00	2.08E+06	'Shrubland'
20.00	0.15	0.95	6.00	3.00	2.08E+06	'Mixed Shrubland/Grassland'
20.00	0.15	0.92	15.00	3.00	2.50E+06	'Savanna'
16.00	0.30	0.93	50.00	4.00	2.50E+06	'Deciduous Broadleaf Forest'
14.00	0.30	0.94	50.00	4.00	2.50E+06	'Deciduous Needleleaf Forest'
12.00	0.50	0.95	50.00	5.00	2.92E+06	'Evergreen Broadleaf Forest'
12.00	0.30	0.95	50.00	4.00	2.92E+06	'Evergreen Needleleaf Forest'
13.00	0.30	0.97	50.00	4.00	4.18E+06	'Mixed Forest'
8.00	1.00	0.98	0.01	6.00	9.00E+25	'Water Bodies'
14.00	0.60	0.95	20.00	6.00	2.92E+06	'Herbaceous Wetland'
14.00	0.35	0.95	40.00	5.00	4.18E+06	'Wooded Wetland'
25.00	0.02	0.90	1.00	2.00	1.20E+06	'Barren or Sparsely Vegetated'
15.00	0.50	0.92	10.00	5.00	9.00E+25	'Herbaceous Tundra'
15.00	0.50	0.93	30.00	5.00	9.00E+25	'Wooded Tundra'
15.00	0.50	0.92	15.00	5.00	9.00E+25	'Mixed Tundra'
25.00	0.02	0.90	10.00	2.00	1.20E+06	'Bare Ground Tundra'
55.00	0.95	0.95	0.10	5.00	9.00E+25	'Snow or Ice'
10.00	0.10	0.97	80.00	3.00	1.89E+06	'Low Intensity Residential '
10.00	0.10	0.97	80.00	3.00	1.89E+06	'High Intensity Residential'
10.00	0.10	0.97	80.00	3.00	1.89E+06	'Industrial or Commercial'

Table 10 - MODIS landuse categories and their physical parameters for ’summer’ season taken from LANDUSE.TBL. Parameters from left to right are: Albedo (ALBD), soil moisture availability (SLMO), surface emissivity (SFEM), roughness length (SFZ0), thermal inertia (THERIN) and surface heat capacity (SFHC).

ALBD	SLMO	SFEM	SFZ0	THERIN	SFHC	Category
12.00	0.30	0.95	50.00	4.00	2.92E+06	'Evergreen Needleleaf Forest'
12.00	0.50	0.95	50.00	5.00	2.92E+06	'Evergreen Broadleaf Forest'
14.00	0.30	0.94	50.00	4.00	2.50E+06	'Deciduous Needleleaf Forest'
16.00	0.30	0.93	50.00	4.00	2.50E+06	'Deciduous Broadleaf Forest'
13.00	0.30	0.97	50.00	4.00	4.18E+06	'Mixed Forests'
22.00	0.10	0.93	5.00	3.00	2.08E+06	'Closed Shrublands'
20.00	0.15	0.95	6.00	3.00	2.08E+06	'Open Shrublands'
22.00	0.10	0.93	5.00	3.00	2.08E+06	'Woody Savannas'
20.00	0.15	0.92	15.00	3.00	2.50E+06	'Savannas'
19.00	0.15	0.96	12.00	3.00	2.08E+06	'Grasslands'
14.00	0.42	0.95	30.00	5.50	3.55E+06	'Permanent wetlands'
17.00	0.30	0.99	15.00	4.00	2.50E+06	'Croplands'
15.00	0.10	0.88	80.00	3.00	1.89E+06	'Urban and Built-Up'
18.00	0.25	0.98	14.00	4.00	2.50E+06	'cropland/natural vegetation mosaic'
55.00	0.95	0.95	0.10	5.00	9.00E+25	'Snow and Ice'
25.00	0.02	0.90	1.00	2.00	1.20E+06	'Barren or Sparsely Vegetated'
8.00	1.00	0.98	0.01	6.00	9.00E+25	'Water'
15.00	0.50	0.93	30.00	5.00	9.00E+25	'Wooded Tundra'
15.00	0.50	0.92	15.00	5.00	9.00E+25	'Mixed Tundra'
25.00	0.02	0.90	10.00	2.00	1.20E+06	'Barren Tundra'

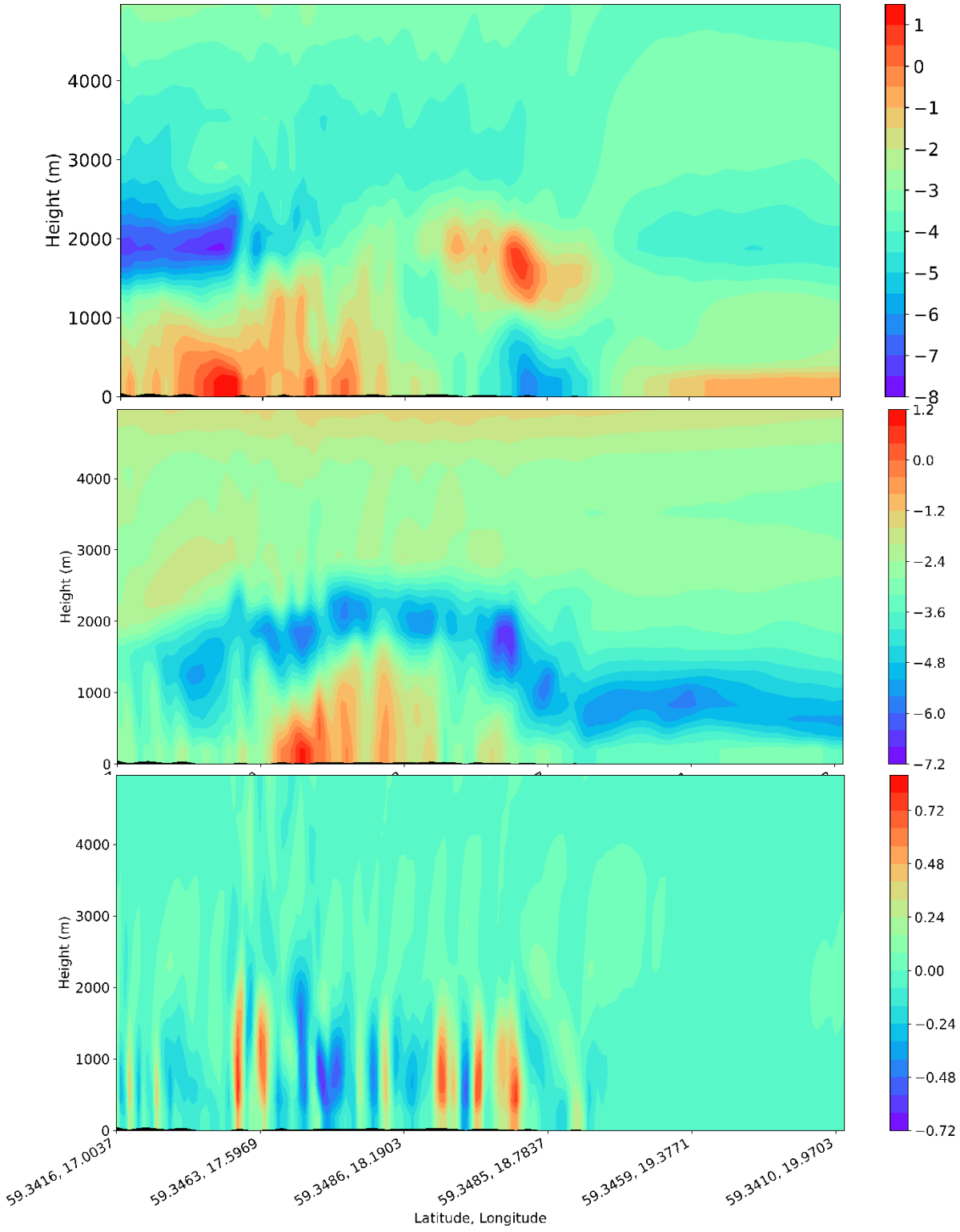

Figure 26 – Vertical cross section for u (top), v (center) and w (bottom) wind components (m/s) from CORINE simulation, along the W-E cross section showed in Figure 7, on the 24th July 12:00 UTC.